

Joint spectroscopic and theoretical investigations of transition metal complexes involving non-innocent ligands†

Kallol Ray,^a Taras Petrenko,^b Karl Wieghardt^{*b} and Frank Neese^{*a}

Received 3rd January 2007, Accepted 5th March 2007

First published as an Advance Article on the web 26th March 2007

DOI: 10.1039/b700096k

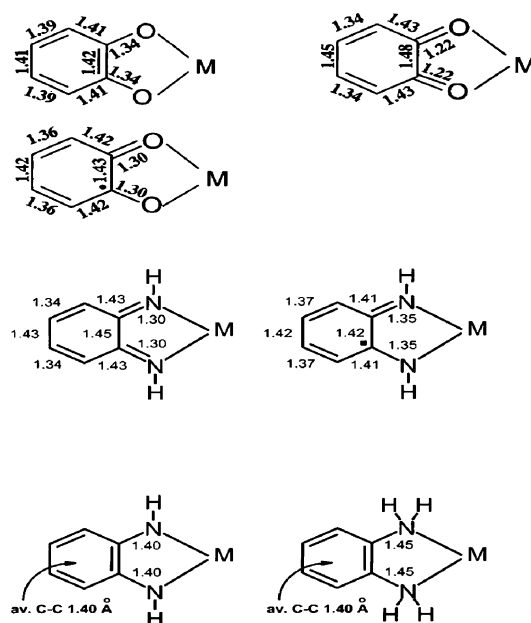
A series of transition metal complexes involving non-innocent *o*-dithiolene and *o*-phenylenediamine ligands has been characterized in detail by various spectroscopic methods like magnetic circular dichroism (MCD), absorption (abs), resonance Raman (rR), electron paramagnetic resonance (EPR), and sulfur K-edge X-ray absorption spectroscopies. A computational model for the electronic structure of the complexes is then proposed based on the density functional theory (DFT) or *ab-initio* methods, which can successfully account for the observed trends in the experimental spectra (MCD, rR, and abs) of the complexes. Based on these studies, the innocent vs non-innocent nature of the ligands in a given transition metal complex is found to be dependent on the position of the central metal ion in the periodic table, its effective nuclear charge in interplay with relativistic effects.

1. Introduction

The interaction of transition metal ions with organic radicals is a subject that currently receives much attention.^{1–3} One of the driving forces for this research direction is the realization that such systems exist in the active sites of metalloproteins.² The best understood example is galactose oxidase which features a single Cu(II) ion coordinated to a modified tyrosyl-radical.¹ It is only due to this intricate bonding situation that the enzyme can perform the specific two-electron oxidation of alcohols to aldehydes. Other examples of such electronic structure contributions to reactivity are expected to be found in biochemistry. However, some of them may be difficult to detect in, for example, the cases where there are two radical ligands which strongly couple through a central metal ion.⁴ Thus, it is important to have a clear understanding of the bonding and physical properties of such complexes if one wants to understand their reactivity. Consequently, a large number of transition metal complexes with one-, two-, or three coordinating radicals have been synthesized in recent years and subjected to detailed physical characterization.^{5–11} In many cases, the complexes studied or closely related compounds have been known since the 1960s (see ref. 7, 8 and references therein). However, it is only recently through a combination of contemporary theory and experiment that their properties become understood.^{7,9,11–13}

X-Ray crystallography has proved to be a useful tool in determining the oxidation level of non-innocent ligands involving oxygen and nitrogen donor atoms.^{6–10} A variety of typical structural features have been identified which allow the unequivocal detection and characterization of O,*O'*-coordinated

o-benzosemiquinonate (1–) or N,N'-coordinated *o*-iminobenzo-semiquinonate (1–) π -radicals in a given coordination compound. Probably the most reliable single feature in this respect is the metrical parameters of such ligand systems in their various oxidation levels as shown schematically in Scheme 1. The situation is however, more complicated in delocalized systems, where the free electron of the radical ligand is shared between one or more ligands.¹⁴ The differences in the metrical parameters for the innocent and non-innocent forms of the ligand, in such cases, are often small and may not be detectable by X-ray crystallography. The same is true for the complexes involving sulfur donor ligands,¹⁵ and hence, as explained earlier,¹⁵ the structural parameters are of only limited value for the identification of the redox state



Scheme 1 Metrical parameters of the ligands.

^aInstitut für Physikalische und Theoretische Chemie, Universität Bonn, Wegelerstrasse 12, D-53115, Bonn, Germany. E-mail: neese@thch.uni-bonn.de; Fax: +49 228 739 064; Tel: +49 228 732 351

^bMax-Planck Institut für Bioanorganische Chemie, Stifstr. 34-36, D-45470, Mülheim an der Ruhr, Germany

† The HTML version of this article has been enhanced with additional colour images.

Dr Kallol Ray was born in Kolkata, India. He received his B.S. degree from St. Xavier's College, Calcutta University, and M.S. degree from the Indian Institute of Technology, Kanpur. He moved to the Max-Planck Institute for Bio-Inorganic Chemistry, Mülheim, Germany, as a PhD student in 2002, and joined the research group of Prof. Dr Karl Wieghardt. During his PhD he was involved in the spectroscopic and density functional characterization of transition metal complexes involving non-innocent ligands. He was awarded the Summa Cum Laude PhD degree on Jan 25th 2006. Presently he is working as a post-doctoral associate on high valent iron oxo complexes in the University of Minnesota under the supervision of Prof. Lawrence Que Jr.

Dr Taras Petrenko was born in Kyiv, Ukraine. He received his M.S. degree in physics from the Taras Shevchenko Kyiv University, Ukraine. He completed his PhD work in solid-state physics under the supervision of Dr V. Ya. Bratus' at the Institute of Semiconductor Physics, Kyiv. In 2003 he joined as a post-doctoral fellow the research group of Prof. Dr Frank Neese at the Max-Planck Institute for Bio-Inorganic Chemistry, Mülheim, Germany. There he was involved in the spectroscopic and quantum chemical characterization of transition metal complexes, and method development for experimental analysis and quantum chemical calculation of optical properties of molecules. Presently he is working as a post-doctoral fellow at the University of Bonn.

Prof. Dr Karl Wieghardt studied chemistry at the universities of Hamburg and Heidelberg where he also completed his PhD work. He spent a year as a post-doctoral fellow with Prof. Sykes in Leeds in 1972 and completed his habilitation at the University of Heidelberg in 1974. Following his appointment as Professor of inorganic chemistry at the University of Hannover, Germany, he became the chair of inorganic chemistry at the Ruhr University Bochum in 1981. Since 1994 he has been a director at the Max-Planck institute for bioinorganic chemistry in Mülheim, Germany. He has made many well-known contributions to coordination- and bioinorganic chemistry that received numerous prestigious awards. His studies range from fundamental aspects of magnetochemistry to biomimetic model chemistry, catalysis and more recently the chemistry and electronic structure of transition metals with coordinating ligand radicals.

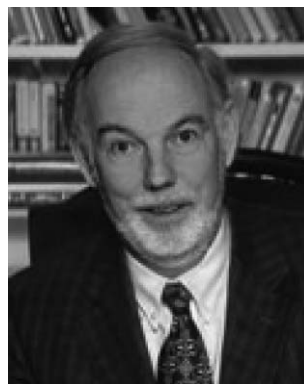
Prof. Dr Frank Neese was born in Wiesbaden, Germany. He received his PhD in biochemistry from the department of biology, University of Konstanz. From 1997–1999 he spent two years as a post-doctoral fellow with Prof. Edward I. Solomon in Stanford, USA. Following his habilitation in 2001 (University of Konstanz), he moved as a group leader to the Max-Planck institute for bioinorganic chemistry in Mülheim, Germany. In 2006 he accepted the chair of theoretical chemistry at the University of Bonn, Germany. His research interests include the electronic structure and spectroscopy of open-shell transition metals in all branches of chemistry and biochemistry as well as the development of new quantum chemical methods that are implemented into the large-scale electronic structure program ORCA that originates from his research group.



Kallol Ray



Taras Petrenko



Karl Wieghardt



Frank Neese

of benzene-1,2-dithiolate or related ligands in a given complex. Understanding the electronic structure of the ground state of such systems is thus a non-trivial problem and insights from sophisticated experiments are a prerequisite for progress in the field.

Here we briefly review a detailed spectroscopic and theoretical study on a number of square based pyramidal $[\text{Cr}(\text{L})_2\text{O}]^{1-}$, and square planar $[\text{M}(\text{L})_2]^{z-}$ ($z = 2-, 1-, 0$; $\text{M} = \text{Fe}, \text{Co}, \text{Ni}, \text{Pd}, \text{Pt}, \text{Cu}, \text{Au}$), and $[\text{Co}(\text{L}_{\text{N,N}})_2]$ complexes, the electronic structures of which have been controversially discussed in the literature¹⁶ {L and $\text{L}_{\text{N,N}}$ refers to the doubly deprotonated forms of the benzene-1,2-dithiol and *o*-phenylenediamine ligands, respectively}. It is shown, how by piecing together the various clues derived from the

a variety of physical methods (*viz* sulfur K-edge X-ray absorption spectroscopy (XAS), resonance Raman (rR), electron paramagnetic resonance (EPR), absorption (abs), and magnetic circular dichroism (MCD)), and their comparison with density functional theoretical (DFT) as well as *ab initio* electronic structure studies, it is possible to generate a coherent picture of the metal binding site. This provides insight into the electronic structure of the metal ion and the ligands that surround it. Based on our studies L and $\text{L}_{\text{N,N}}$ ligands are both found to be capable of undergoing one electron oxidation yielding the dithiobenzosemiquinonato ($1-$), ($\text{L}^{\cdot-}$), and diiminobenzosemiquinonato ($1-$), ($\text{L}_{\text{N,N}}^{\cdot-}$), radical ions, respectively (here we use the following ligand abbreviations: the aromatic dianion, a benzene dithiolato ($2-$), $[\text{C}_6\text{H}_4\text{S}_2]^{2-}$, is

(L^{2-}); its π radical monoanion, a dithiobenzosemiquinonato ($1-$), $[C_6H_4S_2]^{1-}$, is (L^{1-}); the deprotonated benzene dithiol ligand, $[C_6H_4S_2]$, in general without any assignment of ligand oxidation state, L . *o*-Phenylene diamine ligands are also assigned similarly; $L_{N,N}$ refers to the deprotonated *o*-phenylene diamine ligand in general having chemical composition $[C_6H_4(NH)_2]$; ($L_{N,N}^{2-}$) is the dianion $[C_6H_4(NH)_2]^{2-}$, and $L_{N,N}^{1-}$ is $[C_6H_4(NH)_2]^{1-}$. However, the “non-innocent” vs “innocent” nature of the above potential redox active ligands in a given complex is found to be dependent on the position of the central metal ion in the periodic table, its effective nuclear charge, and relativistic effects.

2. Transition metal dithiolenes

The transition metal bound dithiolene complexes are structurally well-defined compounds with relevance to the Mo-pterin-dithiolene cofactor in mononuclear oxotransferases¹⁷ such as xanthine oxidase, sulfite reductase, and DMSO reductase. Understanding the bonding between the metal and the dithiolene ligand can provide insight into structure/function relationships in these metalloenzymes. These complexes are also of importance in reactions with olefins.¹⁸ In this section a detailed spectroscopic investigation of a series of bis(dithiolene) transition metal complexes will be undertaken to make an unambiguous assignment of their electronic structures. For DFT calculations the complexes containing the deprotonated unsubstituted benzene-1,2-dithiols (L) are considered and the results are compared with the experimental data obtained for the complexes involving the same ligand (L) or the deprotonated 3,5-di-tert-butylbenzene-1,2-dithiols (L^{Bu}).^{15a,d,e,f} The electronic structure of the complexes is known to be independent¹⁵ on the substitution pattern of the ligand.

2.1 Electronic structure of the ligand

Before going to the actual complexes it is instructive to have an idea about the electronic structure of the hypothetical bis(benzene-1,2-dithiolato) ligand (L_2^{4-}). The MO diagram obtained from a BP86 DFT calculation^{15c} of the ligand in D_{2h} symmetry is shown in Fig. 1. It features a set of eight orbitals corresponding to symmetry-adapted linear combinations of the sulfur ligand 3p lone pairs. Four of the sulfur 3p orbitals in Fig. 1 are of π -type ($1b_{3g}$, $1b_{1u}$, $1b_{2g}$, and $1a_u$) and the remaining four are of σ -type ($1b_{3u}$, $1b_{1g}$, $1b_{2u}$, and $1a_{1g}$). In a bis(dithiolene) transition metal complex of D_{2h} symmetry (which is the symmetry of all the complexes considered in this review, except $[Cr(L)_2O]^+$, for which a C_s geometry is energetically favoured), the orbitals of *gerade* symmetry, *viz.*, $1b_{3g}$, $1b_{2g}$, $1b_{1g}$, and $1a_{1g}$, can undergo symmetry allowed mixing with the metal based d-orbitals of appropriate symmetry (d_{yz} , d_{xz} , and d_{xy} in D_{2h} symmetry). However, as explained earlier^{15a,e,f} and will be shown later, the innocent vs non-innocent nature of the dithiolene ligand in a bis(dithiolato) complex is controlled mainly by the interaction of the $1b_{2g}$ orbital of the hypothetical bis(benzene-1,2-dithiolato) ligand with that of the metal d_{xz} orbital, which in turn is controlled by the relative energies of the metal- and ligand fragment orbitals.

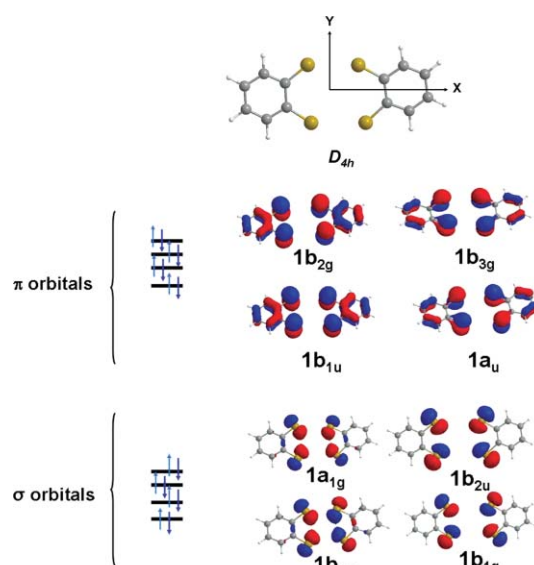


Fig. 1 Molecular orbital scheme of the hypothetical bis(dithiolato) ligand as obtained from BP86 DFT results. For calculation details see ref. 15e.

2.2. Electronic structure of a oxo-bis(benzene-1,2-dithiolato)chromate(v) monoanion

The first transition metal bis(dithiolene) complex that we will consider for our study is $[CrO(L)_2]^{1-}$, which is closely related to the active center of the Molybdo-pterin enzymes,¹⁷ and is also a potential reactive intermediate during the epoxidation of olefins.¹⁸ The crystal structure of the $[CrO(L^{Bu})_2]^{1-}$, (L^{Bu} refers to the deprotonated 3,5-di-tert-butylbenzene-1,2-dithiol ligand) complex, reported earlier in our group,^{15f} shows a symmetry lowering of the molecule from C_{2v} to C_s . From DFT calculation, the C_s instead of C_{2v} symmetry for the complex is attributed to strong $S(3p) \rightarrow Cr(3d_{x^2-y^2})$ π -donation in C_s geometry providing additional stability to the complex.^{15f} The cyclic voltammogram (CV) of $[CrO(L^{Bu})_2]^{1-}$ is reported^{15f} to display a reversible one-electron reduction wave at -0.96 V vs ferrocenium/ferrocene, which is 500 mV lower than what is observed for the corresponding $[MoO(L)_2]^{1-}$ complex.¹⁹ This strong dependence of the reduction potential on the central metal ion is considered as evidence for the predominant metal based oxidation for the $[MO(L^{Bu})_2]^{1-/2-}$ ($M = Cr, Mo$) couple.^{15f}

A. Bonding scheme. The bonding in $[CrO(L)_2]^{1-}$ as shown in Fig. 2 is normal²⁰ with all the Cr 3d orbitals placed at energies much higher than the ligand orbitals, and hence are energetically not available for extensive mixing with the ligand orbitals. Thus the Cr–S covalency within the d-orbital manifold is predicted to be small by the calculations.^{15f} The electronic configuration in $[CrO(L)_2]^{1-}$ is formally $3d^1$ with the unpaired electron residing in the $Cr(3d_{x^2-y^2})$ orbital, which is essentially non-bonding (80% $3d_{x^2-y^2}$). Thus, from the calculations the complex is best represented as $[Cr^VO(L^{2-})_2]^{1-}$, containing fully reduced aromatic benzene dithiolato ($2-$) (L^{2-}) ligands attached to a Cr(V) centre. The intense pre-edge feature at 5991.75 eV in the Cr K-edge spectrum for the $[CrO(L^{Bu})_2]^{1-}$ anion, indeed supports a Cr(V) assignment for the complex.^{15f} The d-orbital splitting, as evident from Fig. 2, is thus predicted to be $3d_{x^2-y^2} < 3d_{xz}, 3d_{yz} < 3d_{xy} < 3d_{z^2}$. This splitting results from the fact that the terminal oxo

ligand is an extremely strong σ - and π -donor, and in the presence of a moderate-to-weak equatorial ligand field, as in the present case, the d-orbital splitting diagram in Fig. 2 results. The $3d_z^2$ and $3d_{xz}, 3d_{yz}$ orbitals are strongly destabilised by σ - and π -antibonding interactions with the terminal oxo ligand to such an extent that they always tend to remain unoccupied.

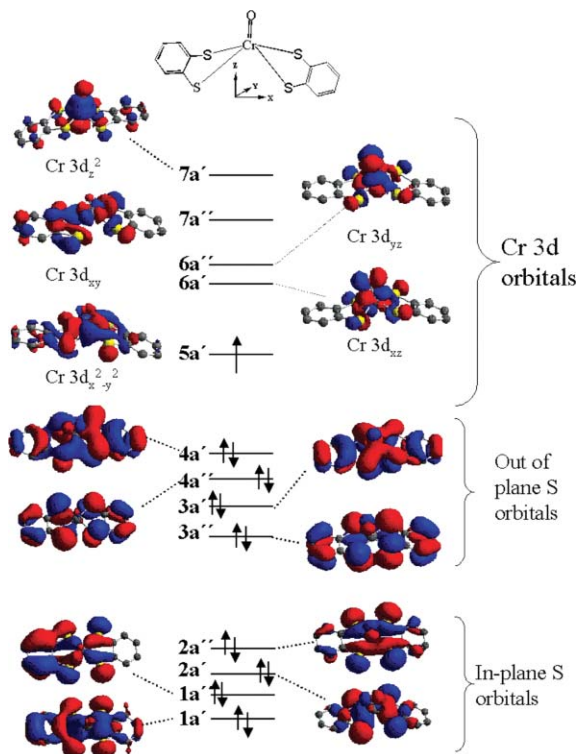


Fig. 2 Kohn–Sham MOs and energy scheme of the $[\text{Cr}^{\text{V}}\text{O}(\text{L}^{1-})_2]^{1-}$ anion as obtained from a spin unrestricted ZORA-B3LYP DFT calculation. Reproduced with permission from ref. 15f.

B. Spectroscopic properties.

1. EPR spectroscopy. The $[\text{Cr}^{\text{V}}\text{O}(\text{L}^{2-})_2]^{1-}$ anion is paramagnetic with a spin doublet, $^2A'$, ground state,^{15f} and hence can be analyzed by EPR spectroscopy. The X-band EPR spectra of $[\text{Cr}^{\text{V}}\text{O}(\text{L}^{\text{Bu}2-})_2]^{1-}$ in frozen CH_2Cl_2 solution^{15f} is characterized by a magnetic anisotropy in the g -tensor ($g_x = 1.98$, $g_y = 1.99$, $g_z = 2.02$).^{15f} The anisotropy in the ^{53}Cr hyperfine splitting, however, could not be resolved within the experimental line width (30 G) of the experiment and an isotropic hyperfine interaction due to the ^{53}Cr ($I = 3/2$) nucleus ($A_{\text{iso}} = 35$ MHz) is obtained from the simulation of the experimental spectrum.^{15f} The observed trend in the g -tensor anisotropy that one principal g -value (g_z) is larger than the free electron g -value, while the two perpendicular components are below it, is unusual for a $\text{Cr}(\text{v})$ d^1 system, where all ligand-field excited states only contribute to negative shifts.¹⁶ⁿ The EPR parameters are thus calculated for the $[\text{Cr}^{\text{V}}\text{O}(\text{L}^{\text{Bu}2-})_2]^{1-}$ ion based on the molecular orbital scheme in Fig. 2, in order to understand the unusual g_z shift in the experimental spectrum. In the calculation the Fermi contact, dipolar and metal spin-orbit contributions to the g and A tensors are included. The calculated values ($g_x = 1.978$, $g_y = 1.986$, $g_z = 2.015$; $A_{\text{iso}} = 23.1$ MHz) are in excellent agreement with the experiment.^{15f} In the calculation, positive g_z shift originates from the spin orbit coupling of the

ground state with the low lying ligand to metal charge transfer excited states (see Section 1B-3).

2. Sulfur K-edge XAS. The sulfur K-edge arises from an electric dipole allowed local $1s \rightarrow 4p$ transition.²¹ In cases where the ligand is bound to a transition metal with a partially filled d-shell the covalent interaction between the ligand 3p-orbitals and the metal 3d-orbitals, produces partial ligand 3p-hole character. This results in a pre-edge transition, the intensity of which will reflect the covalency of the metal–ligand bond.²² Since the intensity of the pre-edge transition is directly related to the extent of metal–ligand covalency, a theoretical sulfur K-edge spectrum can be obtained based on the calculated Cr–S covalencies^{15f} of the singly occupied or the virtual orbitals of the $[\text{Cr}^{\text{V}}\text{O}(\text{L}^{2-})_2]^{1-}$ anion, which can then be compared with the experiment. Fig. 3 shows the theoretical sulfur K-edge spectrum of $[\text{Cr}^{\text{V}}\text{O}(\text{L}^{2-})_2]^{1-}$ in the range 2468–2472 eV, as obtained from time dependent density functional methods. Obviously, the agreement with the experimental spectrum obtained for the $[\text{Cr}^{\text{V}}\text{O}(\text{L}^{\text{Bu}2-})_2]^{1-}$ complex is quite good. Both, the relative intensities and energies of the individual pre-edge transitions (Fig. 3 and ref. 15f) are nicely reproduced by the calculations, and hence the MO diagram shown in Fig. 2 represents the correct ground state of $[\text{Cr}^{\text{V}}\text{O}(\text{L}^{2-})_2]^{1-}$. The details of the calculations are provided in ref. 15f. The broad sulfur K pre-edge feature in $[\text{Cr}^{\text{V}}\text{O}(\text{L}^{\text{Bu}2-})_2]^{1-}$ in the range 2468–2472 eV, based on DFT calculations, is thus attributed to the superposition of five individual pre-edge transitions (Fig. 3) from the sulfur ($1s$) orbital to the five predominantly metal based orbitals ($5a'$, $6a'$, $6a''$, $7a'$, and $7a''$ in Fig. 2) in their covalent interaction with the sulfur 3p-orbitals. The most intense transition in the region of

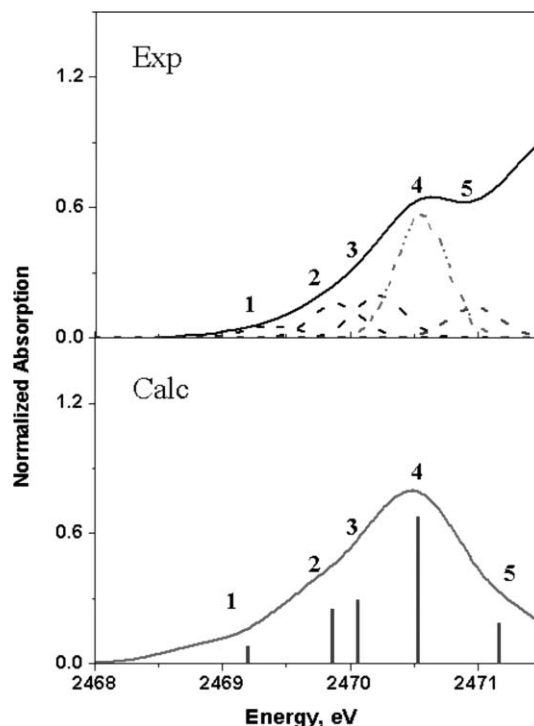


Fig. 3 Deconvoluted sulfur K-edge X-ray absorption spectrum of the $[\text{Cr}^{\text{V}}\text{O}(\text{L}^{\text{Bu}1-})_2]^{1-}$ anion (top) in the pre-edge region and its comparison to that of the calculated sulfur K-edge X-ray absorption spectrum of $[\text{Cr}^{\text{V}}\text{O}(\text{L}^{1-})_2]^{1-}$ anion as obtained from BP86 time-dependent-density functional calculations. Reproduced with permission from ref. 15f.

band 4 (2470.5 eV) is attributed to a transition to the Cr ($3d_{xy}$), ($7a''$) orbital. This orbital is strongly antibonding (35% sulfur 3p character) with the sulfur- σ orbitals and hence features the largest sulfur character of all metal-based MOs.^{15f}

3. *MCD spectroscopy.* Magnetic circular dichroism (MCD) has become an important experimental technique for the investigation of the geometric and electronic structures of transition metal complexes in a variety of areas, perhaps most notably bioinorganic chemistry.^{23,24} In an MCD experiment one measures the differential absorption of left and right circularly polarized light induced in the presence of a longitudinal magnetic field. The theory of MCD spectroscopy has been pioneered by Stephens²⁵ and concisely summarized in an excellent monograph by Piepho and Schatz²⁶ that also discusses the method of moments developed by Henry *et al.*²⁷ and advanced by Stephens and co-workers.²⁸ As the MCD dispersion possesses sign, overlapping bands in absorption spectra are often resolved in the MCD. This is of particular importance in highly covalent systems, as in the dithiolene complexes, as they display multiple, low lying charge transfer transitions that overlap with ligand field bands. A useful measure of the character of the electronic transitions is the oscillator strength obtained from absorption spectroscopy as well as C/D ratios, which reflect the relative intensities of the MCD and absorption features for a given electronic transition. Thus, high oscillator strength ($>10^{-4}$) with small C/D ratios (<0.01) reflect CT transitions, whereas low oscillator strengths ($<10^{-4}$) and high C/D ratios (>0.01) are typically observed for d-d transitions.²⁹ The temperature and field dependence of the MCD signal (VTVH-MCD) contains considerable information regarding the nature of the ground state wavefunction and is therefore complementary to techniques such as EPR and magnetic susceptibility.^{30,15}

The MCD spectrum of the $[\text{Cr}^{\text{VO}}(\text{L}^{\text{Bu}2-})_2]^{1-}$ complex has been recorded at 5 K and 5 T. Simultaneous fit of the absorption spectrum (room temperature) and the MCD spectrum has been performed in order to identify the individual transitions in the range 24000 to 10000 cm^{-1} . This gives rise to a total of seven detectable (bands 1 to 7 in Fig. 4) transitions for $[\text{Cr}^{\text{VO}}(\text{L}^{\text{Bu}2-})_2]^{1-}$ below 24000 cm^{-1} .

Based on their C/D values^{15f} the transitions can be subdivided into two classes. Bands 1 to 4 are characterized by low C/D (large absorption intensity and small MCD intensity) values^{15f} and hence they are assigned to dipole allowed ligand-to-metal charge transfer (LMCT) bands. In contrast, bands 5, 6 and 7 possess comparatively larger C/D (comparable absorption and MCD intensities) ratios^{15f} and are assigned to ligand field transitions. The assignments are corroborated by the results of the TD-DFT calculation performed on the $[\text{Cr}^{\text{VO}}(\text{L}^{2-})_2]^{1-}$ species, based on the MO picture shown in Fig. 2. The low symmetry of $[\text{Cr}^{\text{VO}}(\text{L}^{2-})_2]^{1-}$ makes all transitions from the eight doubly occupied MOs in Fig. 2 into the singly occupied $5a(3d_{x^2-y^2})$ orbital and the four virtual d-based orbitals dipole allowed. However, the allowed transitions are all LMCT in origin. Accordingly, the absorption spectrum of the complex lacks any intense ($>10^4 \text{ M}^{-1} \text{ cm}^{-1}$) intervalence ligand-to-ligand charge transfer transition in the near-infrared region, which has been previously established as a marker band¹⁵ for the presence of dithiobenzosemiquinonate ($1-$) radicals in planar bis-dithiolene coordination complexes. This again confirms the lack of any ligand based redox chemistry for the $[\text{CrO}(\text{L}^{\text{Bu}})_2]^{2-/1-}$ couple.^{15f}

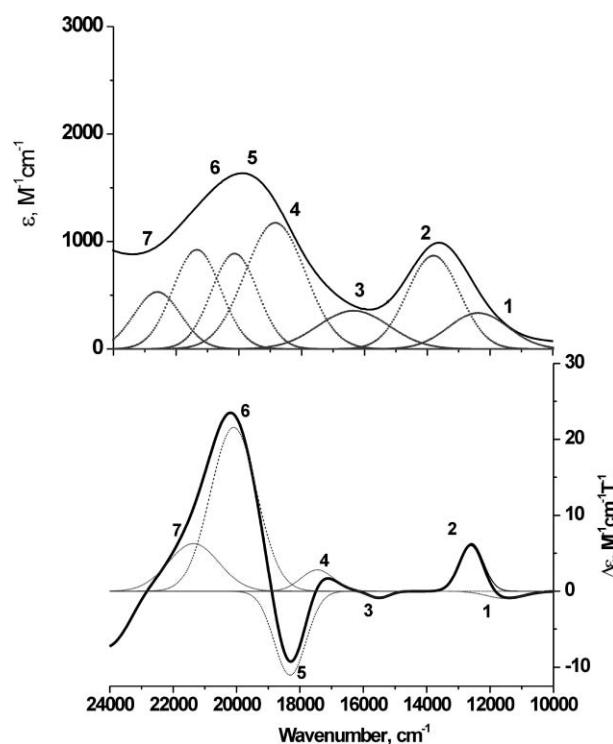


Fig. 4 Deconvoluted room temperature electronic absorption spectrum of the $\text{Cr}^{\text{VO}}(\text{L}^{\text{Bu}1-})_2]^{1-}$ anion (top) and its magnetic circular dichroism (MCD) spectrum (bottom) recorded at 5 K and 5.0 T. Reproduced with permission from ref. 15f.

The calculated transition energies and oscillator strengths are in reasonable agreement with the experimental data.^{15f} The observed signs of the MCD bands are also in full agreement with the assignments based on the sign conventions established for transitions in C_s symmetry.³¹ This again confirms the validity of the calculated MO scheme for the $[\text{Cr}^{\text{VO}}(\text{L}^{2-})_2]^{1-}$ complex. In the calculation the four LMCT bands (bands 1–4) correspond to the transitions from the four out-of-plane sulfur p orbitals of π -symmetry to the singly occupied Cr $3d_{x^2-y^2}$ orbital. The presence of low-lying LMCT excited states explains the principal g -value in the experimental EPR spectrum^{15f} being larger than the free electron g value.

2.3. **Electronic structure of the isoelectronic square planar $[\text{Fe}(\text{L})_2]^{2-}$ and $[\text{Co}(\text{L})_2]^{1-}$.** The next complexes that we consider for our study are the isoelectronic square planar $[\text{Fe}(\text{L})_2]^{2-}$ and $[\text{Co}(\text{L})_2]^{1-}$ complexes, possessing a spin triplet ($S = 1$) ground state. For both the complexes a large zero-field splitting (ZFS) $D = \sim 30 \text{ cm}^{-1}$ has been obtained based on variable temperature and variable field (VTVH) magnetization measurements. Far infrared and VTVH MCD measurements^{15a} done on the $[\text{Co}(\text{L})_2]^{1-}$ complex also support a large zero-field splitting value for the complex in agreement with the VTVH magnetization measurements. The absorption spectra of the above two isoelectronic species are however, found to be significantly different. The $[\text{Co}(\text{L})_2]^{1-}$ complex is deep blue in colour and possesses intense charge transfer bands in the visible, whereas, the $[\text{Fe}(\text{L})_2]^{2-}$ complex is yellow in colour and lacks any intense band in the visible.^{15a} In this section particular efforts are directed toward an understanding

of the origin of the large ZFS and the differences between their absorption spectra in the above two isoelectronic complexes.

A. Bonding scheme. The MO picture obtained from the spin unrestricted B3LYP DFT calculations on the $[\text{Fe}(\text{L})_2]^{2-}$ and $[\text{Co}(\text{L})_2]^{1-}$ complexes are shown in Fig. 5. D_{2h} symmetry has been assumed for the complexes with the coordinate axes as shown in Fig. 5. The ground state for both the complexes is calculated to be $^3\text{B}_{1g}$. For the $[\text{Fe}(\text{L})_2]^{2-}$ complex, the bonding is again normal,²⁰ similar to that in $[\text{Cr}^{\text{V}}\text{O}(\text{L}^{2-})_2]^{1-}$, with all the Fe 3d-orbitals placed at a higher energy relative to the ligand orbitals ($1b_{3g}$, $1a_u$, $1b_{1u}$, and $1b_{2g}$). The energy of the metal 3d-orbitals relative to the ligand orbitals is however, found to be higher in $[\text{Cr}^{\text{V}}\text{O}(\text{L}^{2-})_2]^{1-}$ (see Fig. 16 below) than in $[\text{Fe}(\text{L})_2]^{2-}$. The additional stabilization of the 3d-orbitals in $[\text{Fe}(\text{L})_2]^{2-}$ arises from the higher effective nuclear charge of Fe(II) compared to Cr(II).^{32,33} The relative energies of the Fe 3d-orbitals and the ligand orbitals, are however, still too high to allow for a complete ligand-to-metal electron transfer in $[\text{Fe}(\text{L})_2]^{2-}$. The singly occupied molecular orbitals in $[\text{Fe}(\text{L})_2]^{2-}$ ($2b_{2g}$ and $2b_{3g}$ orbitals in Fig. 5) are thus predominantly metal centred and as explained earlier^{15a} the electronic structure of the complex can be described in terms of a spin triplet d^6 , Fe^{II} , ion attached to two innocent benzene dithiolato ($2-$) ligands. The complex can thus be represented as $[\text{Fe}^{\text{II}}(\text{L}^{2-})_2]^{2-}$.

The situation is however, different for the corresponding $[\text{Co}(\text{L})_2]^{1-}$ complex. Owing to the higher effective nuclear charge of Co(II),^{32,33} the Co 3d-orbitals in $[\text{Co}(\text{L})_2]^{1-}$ undergo a further downshift in energy (see Fig. 5) to such an extent that they are placed at comparable energies to the ligand orbitals. This causes strong metal–ligand mixing in $[\text{Co}(\text{L})_2]^{1-}$ so that the $2b_{2g}$ SOMO possesses equivalent metal and ligand character. Thus, the electronic structure of $[\text{Co}(\text{L})_2]^{1-}$ is more subtle^{15a} and is best represented by the resonance forms $[\text{Co}^{\text{III}}(\text{L}^{2-})(\text{L}^{2-})]^- \leftrightarrow [\text{Co}^{\text{II}}(\text{L}^{\cdot-})(\text{L}^{2-})]^- \leftrightarrow [\text{Co}^{\text{II}}(\text{L}^{2-})(\text{L}^{\cdot-})]^-$.

B. Calculation of properties

In this section the ground and excited state properties of the complexes are calculated based on the MO scheme given in Fig. 5, which are then compared with the experiments in order to judge the authenticity of the calculations.

1. Ground state

The ZFS for both the complexes are calculated to be large and positive in agreement with experiments.^{15a} In DFT the large ZFS in $[\text{Co}(\text{L})_2]^{1-}$ and $[\text{Fe}^{\text{II}}(\text{L}^{2-})_2]^{2-}$ mainly originates from the

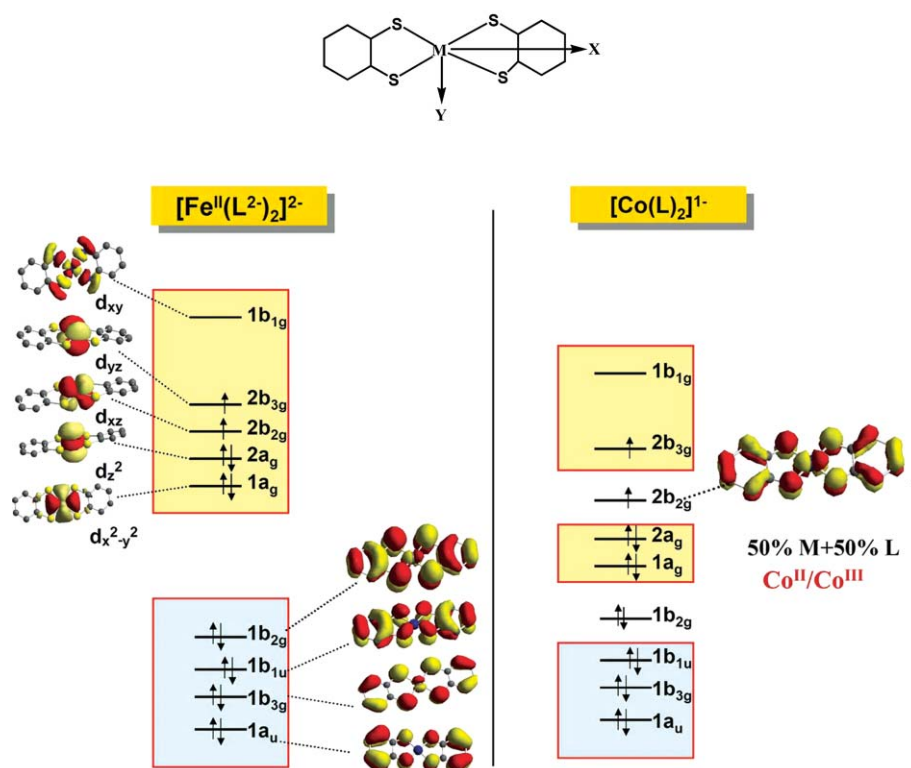


Fig. 5 The molecular orbital picture for the isoelectronic $[\text{Co}(\text{L})_2]^{1-}$ and $[\text{Fe}^{\text{II}}(\text{L}^{2-})_2]^{2-}$ complexes as obtained from a ZORA BP86 DFT calculation. The yellow shaded region represents predominantly metal based orbitals, and the blue shaded region represents predominantly ligand based orbitals. The dominant contribution to the zero-field splitting (ZFS) of the complexes involve the promotion of an electron from the doubly occupied metal based $1a_g$ or $2a_g$ orbitals to the singly occupied $2b_{3g}$ and $2b_{2g}$ orbitals. These excitations take place at comparable energies in the two complexes, as evident from the figure, as all the 3d orbitals on going from $[\text{Fe}^{\text{II}}(\text{L}^{2-})_2]^{2-}$ to $[\text{Co}(\text{L})_2]^{1-}$ are stabilized to the same extent. Hence they possess similar ZFS. However, the LMCT transitions in $[\text{Co}(\text{L})_2]^{1-}$ (transitions from the doubly occupied $1a_u$ or $1b_{1u}$ orbitals to singly occupied $2b_{3g}$ or $2b_{2g}$) takes place at a much lower energy (due to the stabilization of the 3d orbitals) as compared to that in $[\text{Fe}^{\text{II}}(\text{L}^{2-})_2]^{2-}$. Thus, $[\text{Co}(\text{L})_2]^{1-}$ is deep blue in color, whereas, $[\text{Fe}^{\text{II}}(\text{L}^{2-})_2]^{2-}$ is light yellow.

Table 1 Spin and electric dipole allowed transitions possible in the complexes under D_{2h} symmetry

Complex	Spin	Transitions	States	Polarization ^a
[M(L) ₂] ¹⁻ (M = Ni, Pd, Pt)	1/2	1b _{1u} → 2b _{2g}	² B _{2g} (ground state) ² B _{1u}	X
Or		1a _u → 2b _{2g}	² A _u	Y
[Au(L) ₂] ⁰		1a _u → 1b _{1g}	1- ² B _{3u} 2- ² B _{3u}	Z
[M(L) ₂] ²⁻ (M = Ni, Pd, Pt)	0	1a _u → 1b _{1g}	¹ A _g (ground state) ¹ B _{1u}	Z
Or				
[M(L) ₂] ¹⁻ (M = Cu, Au)	0		¹ A _g (ground state)	
[M(L) ₂] ⁰ (M = Ni, Pd, Pt)		1b _{1u} → 2b _{2g}	¹ B _{3u}	X
		1a _u → 2b _{2g}	¹ B _{3u}	Y
		1a _u → 1b _{1g}	¹ B _{1u}	Z
[Co(L) ₂] ¹⁻	1		³ B _{1g} (ground state)	
		1b _{1u} → 2b _{2g}	³ B _{2u}	X
		1b _{1u} → 2b _{3g}	³ B _{3u}	Y
		1a _u → 2b _{2g}	³ B _{3u}	Y
		1a _u → 2b _{3g}	³ B _{2u}	X
		1a _u → 1b _{1g}	³ A _u	Z

^a the intensity of a given transition depends on the direction of polarization. In the present case the X-polarised transitions (along the long axis of the complexes; see Fig. 5 and 10) are most intense and those polarized along Z axis (perpendicular to the molecular plane; see Fig. 5 and 10) are least intense. Y-polarised transitions possess intensities in between.

spin-orbit coupling of the ground state with the low-lying d-d excited states which are found at similar energies in both cases.^{15a} Hence, despite the fact that the Fe 3d-orbitals are placed at a higher energy in [Fe^{II}(L²⁻)₂]²⁻ than the Co 3d-orbitals in [Co(L)₂]¹⁻, the destabilization takes place to a similar extent for all Fe 3d-orbitals (Fig. 5) and, correspondingly, the nature of the d-d excitations are comparable in both species. This is also reflected in the similar magnitude of the *D*-value in both cases.^{15a} In addition to the ZFS, the Mössbauer parameters have also been calculated for the [Fe^{II}(L²⁻)₂]²⁻ species and agreed well with the experimental data.^{15a}

2. Excited state

Under D_{2h} symmetry assumed for the complexes there is a theoretical maximum of five spin and electric dipole allowed transitions from the six doubly occupied MOs in Fig. 5 into the two singly occupied 2b_{2g} and 2b_{3g}, and the virtual 1b_{1g} orbitals. (Table 1). As explained below, each of these transitions (except the 1a_u → 2b_{2g} transition) have been identified in the experimental absorption spectrum of [Co(L^{Bu})₂]¹⁻ based on MCD and resonance Raman (rR) studies. The corresponding [Fe^{II}(L²⁻)₂]²⁻ complex, however proved to be too unstable for MCD or rR measurements.

a. MCD spectra of the cobalt complex. The Gaussian deconvolution of the low-temperature MCD spectrum of [Co(L^{Bu})₂]¹⁻ in butyronitrile together with its room-temperature absorption spectrum in the range 20 000–10 000 cm⁻¹ shows seven detectable individual transitions (Fig 6) for [Co(L^{Bu})₂]¹⁻ below 20 000 cm⁻¹.

In the experimental spectrum, bands 1, 2 and 6 are assigned to ligand field absorptions on the basis of their large *C/D* ratios (> 0.03).^{15a} The presence of these low lying d-d excited states, that can spin-orbit couple with the ground state, accounts for the large zero-field splitting^{15a} measured for the [Co(L^{Bu})₂]¹⁻ species.

Bands 3, 4, 5 and 7 are assigned as charge transfer transitions because of their lower *C/D* ratios. The assignments are

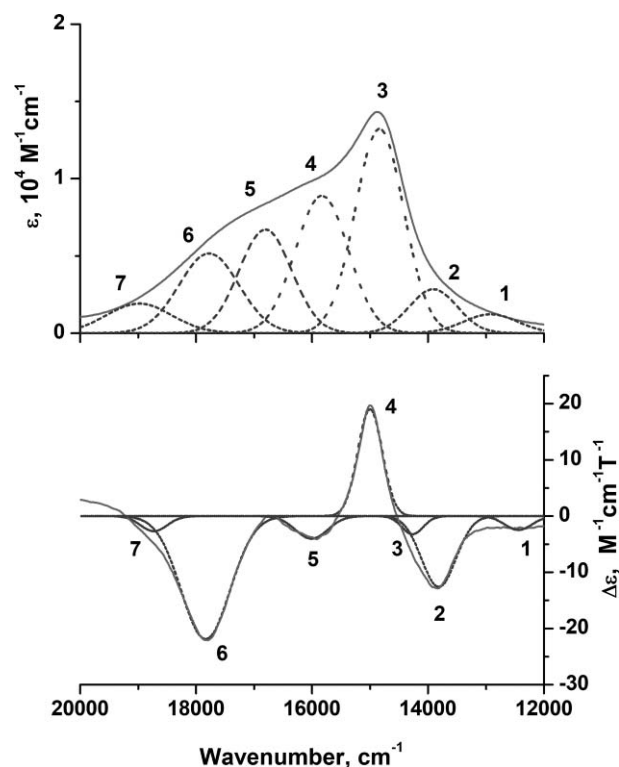


Fig. 6 Deconvoluted room temperature electronic absorption spectrum of [Co(L^{Bu})₂]¹⁻ (top) and its magnetic circular dichroism (MCD) spectrum (bottom) recorded at 32 K and 5.0 T. Reproduced with permission from ref. 15a.

corroborated by the results of the TDDFT calculation performed on the [Co(L)₂]¹⁻ species. The experimental transition energies and oscillator strengths are well reproduced in the calculations,^{15a} thereby confirming the validity of the MO scheme shown in Fig. 5

for the $[\text{Co}(\text{L})_2]^{1-}$ complex. In the calculation the most intense band 3 is $1b_{1u} \rightarrow 2b_{2g}$ in origin and possesses equal intervalence charge transfer (IVCT)¹⁵ and LMCT character. This transition gives the characteristic blue color of the $[\text{Co}(\text{L})_2]^{1-}$ complex.

In $[\text{Fe}^{\text{II}}(\text{L}^{2-})_2]^{2-}$ as explained earlier, the Fe 3d-orbitals are situated high in energy as compared to the ligand orbitals (Fig. 5) owing to the low Z_{eff} of Fe(II). All the spin and electric dipole allowed transitions, occurring in the visible region for the cobalt species are, however, predicted^{15a} to be at much higher energies in the iron case and do not appear among the first 25 states (5500–25 000 cm^{-1} range) in the calculations. Thus, the calculated spectrum for $[\text{Fe}^{\text{II}}(\text{L}^{2-})_2]^{2-}$ does not contain any band of LMCT origin in the 22 000–10 000 cm^{-1} range, in agreement with the experimental data.

b. Resonance Raman spectra of the cobalt complex. Resonance Raman (rR) spectroscopy can selectively probe the vibrational modes of compounds which are in resonance with a given electronic transition. In the resonance region those fundamentals which reflect the change in geometry when converting the molecule from its ground to excited state (Franck–Condon allowed) or those which are able to vibronically couple the resonant excited state to some other electronic state with a different transition moment (Herzberg–Teller allowed) will be strongly enhanced.³⁴ Thus, the correct identification of the vibrational modes showing rR enhancement will aid in the assignment of the electronic transitions and *vice versa*. Moreover, the excited state distortion patterns which can be deduced from a thorough analysis of the rR intensities reflect the electronic and geometric structure of the electronic ground state.

Since all electronic transitions under study are strongly dipole allowed,¹⁵ the totally symmetric modes dominate the rR spectra and reflect the geometry change upon excitation.^{34c} Based on frequency calculations and normal mode analysis,^{15d} the dominant features of the rR spectra for the $[\text{M}(\text{L}^{\text{Bu}})_2]^{1-}$ and $[\text{M}(\text{L})_2]^{1-}$ species are assigned to the five most important, totally symmetric (A_g), rR active vibrational modes ($\nu_{1,2}$, ν_6 , ν_7 and ν_8) as shown in Fig. 7. They represent M–S ($\nu_{1,2}$), C–S (ν_6), or C–C (ν_7 and ν_8) stretches.

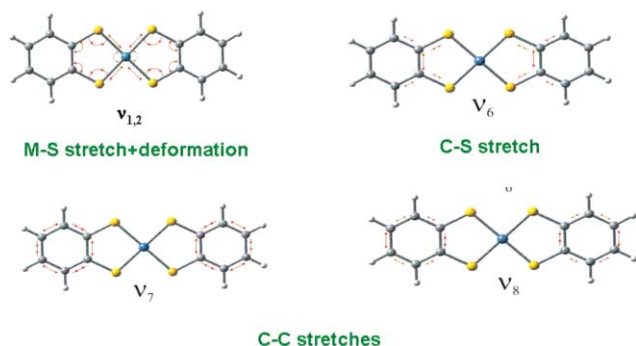


Fig. 7 Totally symmetric fundamentals dominating the resonance Raman spectra of square planar bis(dithiolene) transition metal complexes, as obtained from the frequency calculations and normal mode analysis. For calculation methods see ref. 15d.

The rR spectrum of $[\text{Co}(\text{L}^{\text{Bu}})_2]^{1-}$ with 648 nm (15340 cm^{-1}) excitation presented in Fig. 8 is characterized by the presence of a very intense Raman band at 1268 cm^{-1} , which corresponds to the ν_7 vibrational mode in Fig. 7.^{15d} From the combined fitting of the

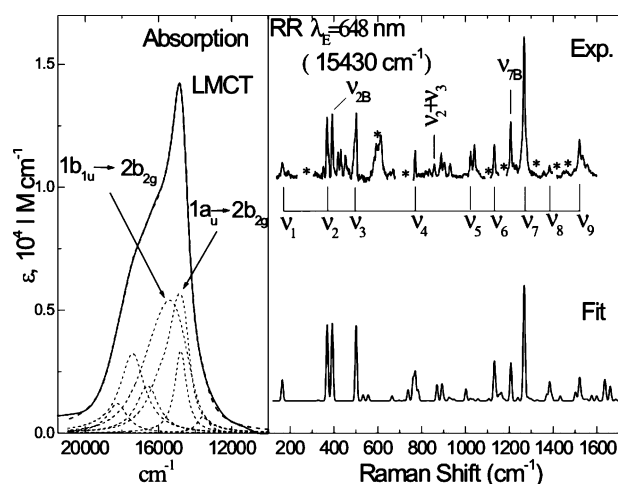


Fig. 8 Deconvoluted absorption spectrum of $[\text{Co}(\text{L}^{\text{Bu}})_2]^{1-}$ in the range 10 000–21 000 cm^{-1} (left); experimental and simulated rR spectra (right) corresponding to dimensionless normal coordinate displacements obtained from the fit (ref. 15d). Artifacts, solvent lines, and spectral regions with removed solvent lines are marked with *. Reproduced with permission from ref. 15d.

rR intensities (upon excitation at 15340 cm^{-1}) and the absorption band shape of the $[\text{Co}(\text{L}^{\text{Bu}})_2]^{1-}$ complex, it is evident (Fig. 7) that the characteristic band in the visible is actually the superposition of seven electronic band systems. The most intense transitions occur at 15 640 cm^{-1} and 15 160 cm^{-1} , respectively. Since, the exciting wavelength (15 340 cm^{-1}) falls in the region of these two bands, both of them must contribute to the observed resonance pattern. These two bands have previously been assigned to $1b_{1u} \rightarrow 2b_{2g}$ and $1a_u \rightarrow 2b_{2g}$ transitions. According to the distortion pattern outlined earlier^{15d} the rR spectrum of the $1b_{1u} \rightarrow 2b_{2g}$ transition in $[\text{Co}(\text{L}^{\text{Bu}})_2]^{1-}$ should be dominated by the ν_6 mode at 1132 cm^{-1} . The difference density plot for the $1a_u \rightarrow 2b_{2g}$ transition, on the other hand, as shown in Fig. 9, shows a pattern of quinoidal distortion, which has the largest projection onto ν_7 . Thus, the $1a_u \rightarrow 2b_{2g}$ transition also contributes to the resonance enhancement of the 1268 cm^{-1} (ν_7) band upon excitation at 15 340 cm^{-1} in $[\text{Co}(\text{L}^{\text{Bu}})_2]^{1-}$. It is to be noted, that the difference

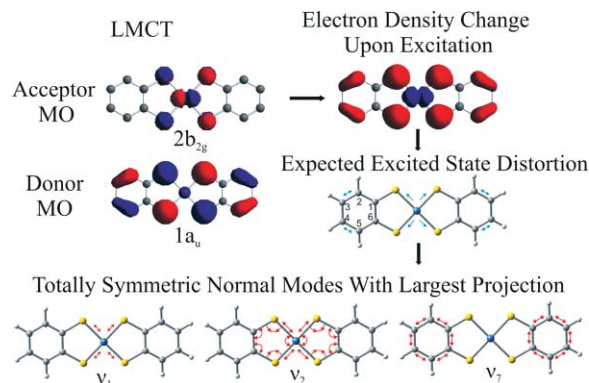


Fig. 9 Normal modes with the largest excited state displacements for the LMCT $1a_u \rightarrow 2b_{2g}$ transition of $[\text{Co}(\text{L})_2]^{1-}$ and their relation to the nature of excitation. Donor and acceptor MOs were obtained from spin-unrestricted BP86 DFT calculations in ref. 15d. Reproduced with permission from ref. 15d.

density plot for a particular transition is highly dependent on the covalency of the donor and acceptor orbitals. Thus, as explained earlier^{15d} and will be shown below, in $[\text{Ni}(\text{L})_2]^{1-}$, where the $2b_{2g}$ level is predominantly ligand based, the Raman spectra upon exciting in the region of the $1a_u \rightarrow 2b_{2g}$ and $1b_{1u} \rightarrow 2b_{2g}$ transitions, show enhancement of the ν_6 mode at $\sim 1100 \text{ cm}^{-1}$. Both the transitions result in a distortion pattern that has maximum displacement along ν_6 and not ν_7 . Thus, the resonance enhancement of the ν_7 band at 1268 cm^{-1} in $[\text{Co}(\text{L}^{\text{Bu}})_2]^{1-}$, upon exciting at 648 nm further corroborates (*vide infra*) the fact that the $2b_{2g}$ level is significantly covalent in $[\text{Co}(\text{L}^{\text{Bu}})_2]^{1-}$, in agreement with the MCD, absorption and DFT results.

2.4. Electronic structure of $[\text{M}(\text{L})_2]^{1-}$ ($\text{M} = \text{Ni}, \text{Pd}, \text{ and Pt}$) complexes

After a successful interpretation of the electronic structure of the $[\text{Cr}^{\text{VO}}(\text{L}^{2-})_2]^{1-}$, $[\text{Fe}^{\text{II}}(\text{L}^{2-})_2]^{2-}$, and $[\text{Co}(\text{L})_2]^{1-}$ complexes, we now consider the electronic structure of the $[\text{M}(\text{L})_2]^{1-}$ ($\text{M} = \text{Ni}, \text{Pd}, \text{ and Pt}$) complexes, which is known to form a three membered electron-transfer series where the neutral species and the dianionic forms are diamagnetic with $S = 0$ ground states whereas the monoanions are paramagnetic ($S = 1/2$). Throughout the past 40 years there has been a debate on the nature of the electronic structure¹⁶ of these complexes. The question of ligand- vs metal-centered redox activity has led to diverse (and sometimes mutually exclusive) descriptions¹⁶ of the electronic structures of the members of an electron-transfer series.

A. Bonding scheme. On the basis of our systematic spectroscopic and theoretical investigations on the $[\text{Cr}^{\text{VO}}(\text{L}^{2-})_2]^{1-}$, $[\text{Fe}^{\text{II}}(\text{L}^{2-})_2]^{2-}$, and $[\text{Co}(\text{L})_2]^{1-}$ complexes, we have learnt that on increasing the Z_{eff} of the central metal ion we lower the energy of the metal d orbitals relative to the ligand orbitals. Thus we arrive from a normal bonding situation as in $[\text{CrO}(\text{L})_2]^{1-}$, and $[\text{Fe}(\text{L})_2]^{2-}$ where the metal 3d-orbitals are all placed at higher energies relative to the ligand, to a situation, as in $[\text{Co}(\text{L})_2]^{1-}$, where the metal and ligand orbitals are placed at comparable energies. If we increase the Z_{eff} of the transition metal ion further, as in $[\text{M}(\text{L})_2]^{1-}$ ($\text{M} = \text{Ni}, \text{Pd}$ and Pt),³²⁻³³ we should now expect an inverted bonding²⁰ situation for the complex, where the metal 3d-orbitals will be placed at lower energies as compared to the ligand orbitals. This situation then leads to an intra-molecular redox reaction and electron transfer from the ligand to the metal. This is indeed found to be the case as shown in the calculated MO scheme (Fig. 10) for the $[\text{Ni}(\text{L})_2]^{1-}$, where the metal based orbitals *viz* $1a_g$ ($d_{x^2-y^2}$), $2a_g$ ($d_{x^2-y^2}$), $1b_{3g}$ (d_{yz}) and $1b_{2g}$ (d_{xz}) are all found at lower energies corresponding to the ligand based orbitals ($1a_u$, $1b_{1u}$, $2b_{2g}$, and $2b_{3g}$). The $2b_{2g}$ SOMO in $[\text{Ni}(\text{L})_2]^{1-}$ is however, in close proximity to the Ni d_{xz} orbital energetically, and hence can undergo a symmetry allowed mixing with it. This results in 30% of Ni $3d_{xz}$ character in the predominantly ligand based $2b_{2g}$ SOMO in $[\text{Ni}(\text{L})_2]^{1-}$.^{15e}

The calculated electronic structure of the isoelectronic $[\text{Pd}(\text{L})_2]^{1-}$ and the $[\text{Pt}(\text{L})_2]^{1-}$ complexes are very similar to that of $[\text{Ni}(\text{L})_2]^{1-}$. However, the back bonding interaction^{15e} of the metal d_{xz} orbital with the ligand $2b_{2g}$ level in the complexes is found to be dependent on the nature of the transition metal ion and decreases in the order $[\text{Ni}(\text{L})_2]^{1-} > [\text{Pt}(\text{L})_2]^{1-} > [\text{Pd}(\text{L})_2]^{1-}$ due to the combined effect of effective nuclear charge and relativistic effects.³⁵ Nevertheless, the $2b_{2g}$ SOMO is predominantly ligand^{15e} based in all the

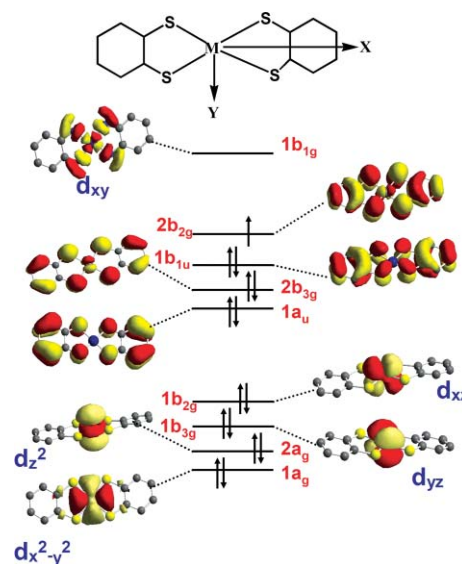


Fig. 10 Kohn-Sham MOs and energy scheme of $[\text{Ni}^{\text{II}}(\text{L}^{2-})(\text{L}^{1-})]^{1-}$ complex from a spin unrestricted ZORA-B3LYP DFT calculation in ref. 15e.

$[\text{M}(\text{L})_2]^{1-}$ ($\text{M} = \text{Ni}, \text{Pd}$ and Pt) complexes and correspondingly the electronic structure of these complexes can be best described as $[\text{M}^{\text{II}}(\text{L}^{2-})(\text{L}^{1-})]^{1-}$, where a d^8 , M^{II} ($\text{M} = \text{Ni}, \text{Pd}$ and Pt) ion is attached to both the dithiobenzosemiquinonato ($1-$) and dithiolato ($2-$) forms of the ligand.^{15e} This is in contrast to the $[\text{Cr}^{\text{VO}}(\text{L}^{2-})_2]^{1-}$, $[\text{Fe}^{\text{II}}(\text{L}^{2-})_2]^{2-}$, and $[\text{Co}(\text{L})_2]^{1-}$ complexes, where the $2b_{2g}$ SOMO was either predominantly metal based, as in $[\text{Cr}^{\text{VO}}(\text{L}^{2-})_2]^{1-}$ and $[\text{Fe}^{\text{II}}(\text{L}^{2-})_2]^{2-}$, or contained equal metal and ligand character ($[\text{Co}(\text{L})_2]^{1-}$).

B. Spectroscopic properties.

1. EPR spectroscopy. The $[\text{M}^{\text{II}}(\text{L}^{2-})(\text{L}^{1-})]^{1-}$ complexes are paramagnetic with a ${}^2B_{2g}$ ground state. Hence they can be characterized by EPR. The X-band rhombic EPR spectrum of $(\text{AsPh}_4)[\text{Ni}^{\text{II}}(\text{L}^{\text{Bu}^{2-}})(\text{L}^{\text{Bu}^{1-}})]$ in CHCl_3/DMF solution has been reported.¹⁶ⁱ $g_1 = 2.18$; $g_2 = 2.04$; $g_3 = 2.01$. By using a ${}^{61}\text{Ni}$ -enriched sample, hyperfine coupling with the ${}^{61}\text{Ni}$ ($I = 3/2$) nucleus was observed: $A_1({}^{61}\text{Ni}) = 16$, $A_2({}^{61}\text{Ni}) < 5$, and $A_3({}^{61}\text{Ni}) = 40 \text{ MHz}$. The X-band EPR spectrum of $[\text{Pt}^{\text{II}}(\text{L}^{\text{Bu}^{2-}})(\text{L}^{\text{Bu}^{1-}})]^{1-}$ in CH_2Cl_2 solution at 10 K shows a rhombic signal with $g = 2.21, 2.06, \text{ and } 1.80$ and a hyperfine coupling to the ${}^{195}\text{Pt}$ ($I = 3/2$; 33% abundance) with $A_{xx} = 320 \text{ MHz}$, $A_{yy} = 278 \text{ MHz}$, and $A_{zz} = 227 \text{ MHz}$.^{15e} The EPR spectrum of $[\text{Pd}^{\text{II}}(\text{L}^{\text{Bu}^{2-}})(\text{L}^{\text{Bu}^{1-}})]^{1-}$ complex,^{15e} in contrast, does not display ${}^{105}\text{Pd}$ ($I = 5/2$; 25% abundance) hyperfine coupling. An isotropic signal at $g_{\text{iso}} = 2.02$ is observed. In order to rationalize the trends in the g - and A -tensors in the complexes EPR spectra of the complexes are calculated based on the MO scheme shown in Fig. 10.

As shown above, all of the $[\text{M}^{\text{II}}(\text{L}^{2-})(\text{L}^{1-})]^{1-}$ species possess a common ${}^2B_{2g}$ ground state with an unpaired electron in the predominantly ligand-based $2b_{2g}$ orbital. Since this SOMO transforms “gerade” upon inversion, it can mix with the out-of-plane metal d_{xz} orbital whereby it acquires some metal character. This metal character gives rise to sizable first-order dipolar metal hyperfine coupling. It also enhances the spin-polarization of the metal core which is responsible for the isotropic Fermi contact contribution to the hyperfine coupling constant. Furthermore,

the $^2B_{2g}$ ground state readily mixes with relatively low-lying d-d excited states thereby giving rise to a sizable orbital angular momentum which contributes to the hyperfine coupling as well as to the g -shifts in the EPR spectra. In the calculation all three contributions to the g - and A -tensors are considered. They are of comparable magnitude in the $[M^{II}(L^{2-})(L^{1-})]^{1-}$ complexes but partially cancel out each other.^{15e} The calculated EPR parameters for the $[Ni^{II}(L^{2-})(L^{1-})]^{1-}$ ($g_1 = 2.18$; $g_2 = 2.07$; $g_3 = 2.02$ and $A_1(^{61}Ni) = 32$, $A_2(^{61}Ni) = -25$, and $A_3(^{61}Ni) = -37$ MHz) and $[Pd^{II}(L^{2-})(L^{1-})]^{1-}$ ($g_1 = 2.04$; $g_2 = 2.05$; $g_3 = 1.98$ and $A_1(^{105}Pd) = 11$, $A_2(^{105}Pd) = 37$, and $A_3(^{105}Pd) = 11$ MHz) complexes are found to be in excellent agreement with the experiments.^{15e} It is important to note that the size of the hyperfine constants are not available from the experiments and hence cannot be directly compared with the DFT results. For the $[Pt^{II}(L^{2-})(L^{1-})]^{1-}$ species the calculated ^{195}Pt hyperfine splittings (-302 , -210 , and -129 MHz) are in acceptable agreement with experiment, but the calculated g_y (2.13) and g_z (1.91) components are somewhat under- and overestimated, respectively, probably reflecting the limitations of the simple semiempirical spin-orbit operator used in this study.^{15e}

2. Absorption spectra. Under D_{2h} symmetry assumed for the complexes, all the spin and electric dipole allowed transitions, together with the corresponding excited states, are summarized in Table 1. The electronic spectra of the $[M^{II}(L^{2-})(L^{1-})]^{1-}$ ($M = Ni, Pd, Pt$) complexes are characterized by very intense absorptions at low energy in the visible region.^{15e} These strong absorptions are entirely absent in the spectra of the one electron reduced dianionic $[M^{II}(L^{2-})_2]^{2-}$ ($M = Ni, Pd,$ and Pt) indicating that their electronic structure is distinctly different from those of the more oxidized species.^{15e} Upon one electron oxidation the low energy transition undergoes a blue shift with the near doubling of intensity.^{15e} The principal absorption at low energy in the monoanionic $[M^{II}(L^{2-})(L^{1-})]^{1-}$ complexes is assigned^{15e} to the ligand-to-ligand intervalence charge transfer (IVCT) $1b_{1u} \rightarrow 2b_{2g}$ (X-polarized) transition (band 1 in Fig. 11). The allowed $1a_u \rightarrow 1b_{2g}$ transition (band 2 in Fig. 11) is also IVCT in origin and occurs at a low energy but with a much lower intensity (Y-polarized). The next allowed transition is a high energy $1a_u \rightarrow 1b_{1g}$ ligand-to-metal charge transfer (LMCT) band and is observed in the UV region.^{15e}

The presence of intense ligand-to-ligand IVCT bands in the near infrared region is thus a spectroscopic marker for the presence of ligand based radicals.¹⁵ The transition energies corresponding to these bands are however, highly dependent on the nature of the central metal ion and shows a trend of decreasing transition energies and increasing intensities on going from the Ni to the Pt and to the Pd species (Fig. 11). To understand the origin of this dependence we need to consider the factors that contribute to the relative energies of the donor and the acceptor orbitals in the IVCTs. The main reason for the splitting of the $1b_{1u}$ and the $2b_{2g}$ orbitals can be attributed to the interaction of the ligand b_{2g} combination with the metal- d_{xz} orbital. Because the combination is antibonding, this interaction raises the energy of the $2b_{2g}$ orbital with respect to the $1b_{1u}$ orbital. In the inverted bonding scheme (Fig. 10), as in the present case, increase in energy of the metal d orbitals will bring them closer to the ligand orbitals. Thus, the super-exchange through the central metal ion will be more effective leading to higher destabilization of the $2b_{2g}$ level with respect to the $1b_{1u}$ and the $1a_u$ levels. Correspondingly, a blue shift in the IVCTs is expected. In the present case, due to the combined variation of the

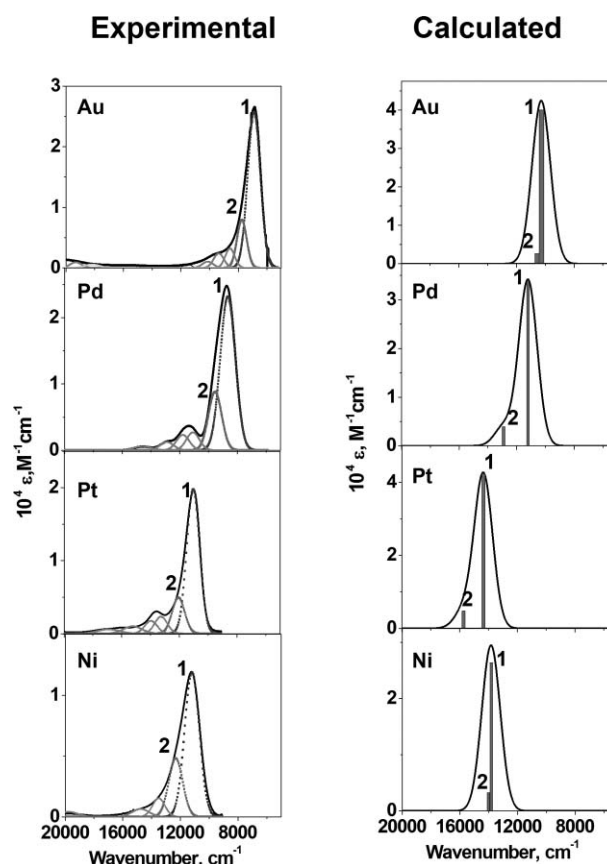


Fig. 11 Experimental and calculated absorption (scalar relativistic-ZORA TD-DFT methods) spectrum for the $[M^{II}(L^{2-})(L^{1-})]^{1-}$ ($M = Ni, Pd$ and Pt) and $[Au^{III}(L^{2-})(L^{1-})]$ species. The experimental values are given for complexes containing 3,5-di-tert-butylbenzenedithiol ligand.

effective nuclear charge and the relativistic effects³⁵ for the central metal ion the energies of the 'nd' orbitals increase as the metal ions are varied in the following order: $Pd < Pt < Ni$. Accordingly, the calculated absorption spectra for the $[M^{II}(L^{2-})(L^{1-})]^{1-}$ ($M = Ni, Pd$ and Pt) species, demonstrate the increasing blue shift of the IVCTs on going from the Pd to Pt and the Ni case, in agreement with the experimental findings (Fig. 11).

In Fig. 11 the neutral $[Au^{III}(L^{2-})(L^{1-})]$ complex has also been included, which is found to have the same electronic structure as the $[M^{II}(L^{2-})(L^{1-})]^{1-}$ ($M = Ni, Pd$ and Pt) complexes based on ^{197}Au Mössbauer and EPR studies.^{15c} The IVCT band in this case is mostly red shifted indicating a very low metal content (10% from ref. 15e) in the $2b_{2g}$ level. This again can be explained on the basis of large Z_{eff} of $Au(III)$ ion³⁵ which makes the $Au(5d_{xz})$ orbital unavailable for any back bonding interaction with the ligand.

3. Resonance Raman spectra. Resonance Raman spectra have been obtained for the complexes corresponding to IVCT and LMCT excitations. As shown in Fig. 12 the enhancement pattern for a LMCT band differs dramatically from an IVCT band in the rR spectra for the $[Ni^{II}(L^{2-})(L^{1-})]^{1-}$ complex. While the former is dominated by moderately enhanced low frequency bands ($\nu_{1,2}$) ($150\text{--}700\text{ cm}^{-1}$), the latter is dominated by rich vibrational peaks above 1000 cm^{-1} . The most intense band upon laser excitation into the IVCT band occurs at $\sim 1100\text{ cm}^{-1}$ (ν_6), which undergoes very little enhancement upon LMCT excitation. These characteristic

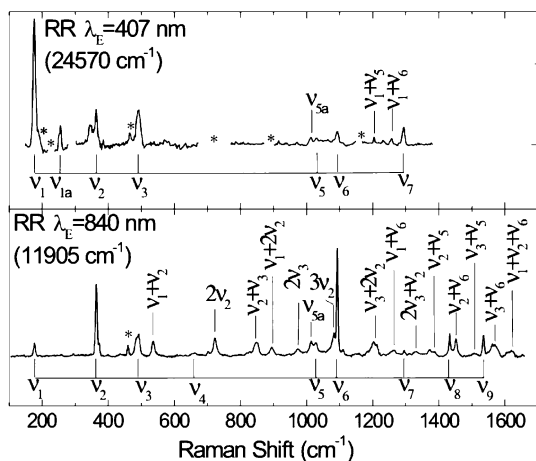


Fig. 12 Comparison of rR spectra of $[\text{Ni}^{\text{II}}(\text{L}^{2-})(\text{L}^{*-})]^{1-}$ complex upon 407 and 840 nm laser excitation (concentration 5.4×10^{-3} M). Artifacts, solvent lines, and spectral regions with removed solvent lines are marked with asterisks. Reproduced with permission from ref. 15d.

features of rR patterns for both types of electronic transitions are preserved in the case of the $[\text{M}^{\text{II}}(\text{L}^{2-})(\text{L}^{*-})]^{1-}$ ($\text{M} = \text{Pd}, \text{Pt}$) and $[\text{M}^{\text{II}}(\text{L}^{\text{Bu}2-})(\text{L}^{\text{Bu}*1-})]^{1-}$ ($\text{M} = \text{Ni}, \text{Pt}$) complexes $\{\text{L}^{\text{Bu}}$ refers to the deprotonated 3,5-di-tert-butylbenzene-1,2-dithiol ligand and L is the corresponding unsubstituted benzene-1,2-dithiol).^{15d} It is important to note that the rR spectra for the complexes are independent of the substitution pattern of the ligand. This is unlike the infrared results which are reported to be strongly dependent on the ligand substitution.^{15d}

The combined fitting of the rR intensities (upon IVCT excitation at 11900 cm^{-1}) and absorption band shape of the $[\text{Ni}^{\text{II}}(\text{L}^{2-})(\text{L}^{*-})]^{1-}$ complex, as done previously for the $[\text{Co}(\text{L}_2)]^{1-}$ complex, shows that the characteristic near IR band is actually the superposition of two electronic band systems. The same is true for all the $[\text{M}^{\text{II}}(\text{L}^{2-})(\text{L}^{*-})]^{1-}$ ($\text{M} = \text{Ni}, \text{Pd}$ and Pt) complexes^{15d} and is consistent with the previous assignment based on TDDFT calculations;^{15e} the two components of the near IR bands corresponding to the $1b_{1u} \rightarrow 2b_{2g}$ and $1a_u \rightarrow 2b_{2g}$ transitions, respectively. The wavelength for IVCT excitation falls in the region of the above two transitions and hence both of them must contribute to the observed excitation features in the rR spectrum of the complex.

In order to understand the excitation pattern in the rR spectra upon IVCT excitation the difference density plot for the $1b_{1u} \rightarrow 2b_{2g}$ and $1a_u \rightarrow 2b_{2g}$ transitions, have been calculated from TDDFT using the bonding scheme shown in Fig. 10. Both of these transitions, show a distortion pattern,^{15d} that has maximum projection along ν_6 mode, as shown in Fig. 13 for the $1b_{1u} \rightarrow 2b_{2g}$ transition. This explains the preferential enhancement of the ν_6 mode at $\sim 1100 \text{ cm}^{-1}$ containing significant C–S stretching character in the rR spectra upon IVCT excitation.

The wavelength for the LMCT excitation falls in the region of $1a_u \rightarrow 1b_{1g}$, the distortion pattern of which shows maximum projection onto $\nu_{1,2}$ modes (Fig. 14). Accordingly the rR spectra of the complex upon LMCT excitation features low frequency bands which are M–S stretch in origin (Fig. 12 and 14), in total contrast to the rR enhancement of C–S stretches at $\sim 1100 \text{ cm}^{-1}$ upon IVCT excitation.

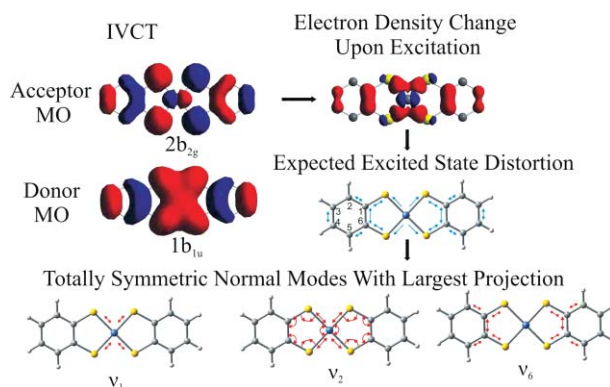


Fig. 13 Normal modes with the largest excited state displacements for the LMCT $1b_{1u} \rightarrow 2b_{2g}$ transition of $[\text{Ni}^{\text{II}}(\text{L}^{2-})(\text{L}^{*-})]^{1-}$ and their relation to the nature of excitation. Donor and acceptor MOs were obtained from spin-unrestricted BP86 DFT calculations in ref. 15d. Reproduced with permission from ref. 15d.

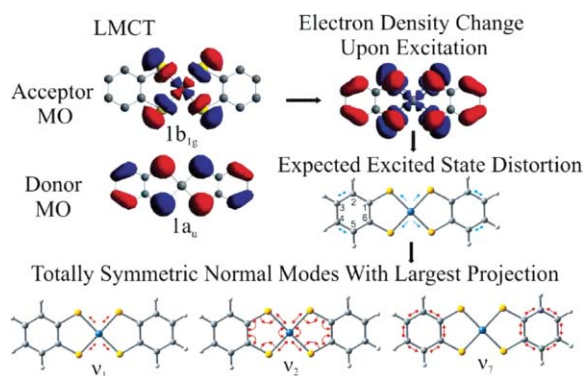


Fig. 14 Normal modes with the largest excited state displacements for the LMCT $1a_u \rightarrow 1b_{1g}$ transition of $[\text{Ni}(\text{L}_2)]^{1-}$ and their relation to the nature of excitation. Donor and acceptor MOs were obtained from spin-unrestricted BP86 DFT calculations in ref. 15d. Reproduced with permission from ref. 15d.

2.5. Electronic structure of $[\text{M}(\text{L}_2)]^{1-}$ ($\text{M} = \text{Cu}, \text{Au}$).

In $[\text{M}(\text{L}_2)]^{1-}$ ($\text{M} = \text{Cu}, \text{Au}$) complexes the $2b_{2g}$ orbital is doubly occupied with an electronic configuration of $(1a_g)^2(2a_g)^2(1b_{3g})^2(1b_{2g})^2(1a_u)^2(2b_{3g})^2(1b_{1u})^2(2b_{2g})^2(1b_{1g})^0$ (the MO scheme shown in Fig. 10 is also valid in this case). Due to the double occupancy of the redox active $2b_{2g}$ orbital the electronic structure of the complexes is best represented as $[\text{M}^{\text{III}}(\text{L}^{2-})_2]^{1-}$ ($\text{M} = \text{Cu}, \text{Au}$). The increasing Z_{eff} of the Cu(II) ion as compared to Ni(II)^{32–33} results in the further stabilization of the Cu 3d orbitals relative to the ligand orbitals in $[\text{Cu}^{\text{III}}(\text{L}^{2-})]^{1-}$, which lowers the back bonding interaction between the Cu d_{xz} and the ligand $2b_{2g}$ orbitals. This is reflected in a 67% decrease in the M–S covalency of the $2b_{2g}$ orbital on going from $[\text{Ni}^{\text{II}}(\text{L}^{2-})(\text{L}^{*-})]^{1-}$ to $[\text{Cu}^{\text{III}}(\text{L}^{2-})_2]^{1-}$.^{15e} The effective nuclear charge increases further on going to the $[\text{Au}^{\text{III}}(\text{L}^{2-})_2]^{1-}$ complex and an additional 20% lowering in the M–S covalency in the $2b_{2g}$ level is observed.^{15e} However, despite the high effective nuclear charge of the central Cu^{II} or Au^{II} oxidation of the ligand does not occur for the $[\text{M}(\text{L}_2)]^{2-/1-}$ ($\text{M} = \text{Cu}, \text{Au}$) couple, as the only possible orbital at the metal that can lose an electron in $[\text{M}^{\text{II}}(\text{L}^{2-})_2]^{2-}$ ($\text{M} = \text{Cu}, \text{Au}$) is the d_{xy} based $1b_{1g}$ orbital, giving rise to a $[\text{M}^{\text{III}}(\text{L}^{2-})_2]^{1-}$ ($\text{M} = \text{Cu}, \text{Au}$) species. The electronic structure of these complexes can thus

best be described in terms of a d^8 Cu^{III} or Au^{III} ion attached to two completely reduced aromatic benzene-1,2-dithiolato dianions.

The double occupancy of the $2b_{2g}$ level in $[\text{M}^{\text{III}}(\text{L}^{2-})_2]^{-}$ ($\text{M} = \text{Cu}, \text{Au}$) complexes results in the absence of any low lying IVCT bands in the near IR region. This band, however, appears upon one electron oxidation as observed for the corresponding $[\text{Au}(\text{L}_2)]$ complex, which is best represented as $[\text{Au}^{\text{III}}(\text{L}^{2-})(\text{L}^{\cdot-})]$.^{15b,e} The electron is lost from the $2b_{2g}$ level and the electronic structure of the oxidized product is similar to that in the $[\text{M}^{\text{II}}(\text{L}^{2-})(\text{L}^{\cdot-})]^{-}$ ($\text{M} = \text{Ni}, \text{Pd}$ and Pt) complexes, with a $^2B_{2g}$ ground state.^{15b,e}

The absorption spectrum of the monoanionic copper complex, $[\text{Cu}^{\text{III}}(\text{L}^{2-})_2]^{-}$, is dominated by an intense charge transfer transition at $24\,616\text{ cm}^{-1}$, which has been identified as $1a_u \rightarrow 1b_g$ LMCT transition.^{15e} As expected the rR spectrum^{15d} upon excitation at $24\,570\text{ cm}^{-1}$ is dominated by low frequency bands having metal–sulfur stretching character, similar to that for the $[\text{Ni}^{\text{II}}(\text{L}^{2-})(\text{L}^{\cdot-})]^{-}$ complex upon UV excitation. This further corroborates the Cu^{III} assignment of the electronic structure of the complex.

3. Electronic structure of bis(*o*-phenylenediamine) cobalt complex

From the previous sections we know that the redox-properties of the bis(dithiolene) transition metal complexes slowly change from being predominantly metal-based to predominantly ligand based on moving from Cr to Ni along the first transition metal ion series. Cobalt represents the extreme case where the metal and ligand orbitals are situated at comparable energies and it is not possible to discern between metal and ligand based chemistry. However, if the effective nuclear charge of the ligand in the Co complex is reduced then the ligand orbitals should undergo a destabilisation in energy, and possess energy higher than the $\text{Co}(3d)$ orbitals. Ligand based redox processes should prevail in such a case. Since the nitrogen $2p$ -orbitals experience a lower effective nuclear charge than the sulfur $3p$ -orbitals it may be possible to reduce the effective nuclear charge of the ligand by moving to ligands involving nitrogen donors instead of sulfurs.

In this section the electronic structure of the neutral $[\text{Co}(\text{L}_{\text{NN}})_2]$ (L_{NN} represents the doubly deprotonated *o*-phenylenediamine ligand) complex is considered in detail by spectroscopic and *ab initio* methods, which is then compared with the electronic structure of the monoanionic $[\text{Co}(\text{L}_2)]^{-}$ species, obtained earlier. The $[\text{Co}(\text{L}_{\text{NN}})_2]^{-}$ complex, which would be more relevant for comparative purposes, unfortunately proved to be too unstable for any spectroscopic studies. The calculations are performed for the $[\text{Co}(\text{L}_{\text{NN}})_2]$ complex and the results are compared with the experimental values (EPR, MCD, and absorption) obtained for the $[\text{Co}(\text{L}_{\text{NN}})_2]$ complex, where $^2\text{L}_{\text{NN}}$ represents the doubly deprotonated *N*-phenyl-*o*-phenylenediamine ligand. It is shown that by moving to nitrogen donor ligands, as in *o*-phenylenediamine, it is indeed possible to initiate a predominantly ligand based redox process in the $[\text{Co}(\text{L}_{\text{NN}})_2]$ complex.

A. Bonding

As explained earlier¹⁴ the description of the neutral $[\text{Co}(\text{L}_{\text{NN}})_2]$ complex in terms of a single-determinant wavefunction, as in DFT, is an oversimplification, and a multiconfigurational *ab initio* treatment is warranted in order to gain insight into its electronic proper-

ties. This is because the ground state wavefunction of the complex contains three open shell $S = 1/2$ fragments which are coupled to a total spin of $S_t = 1/2$. It is clear that such a complicated behaviour can only be crudely modelled with DFT methods.¹⁴ In fact the DFT value of 1.14 unpaired electrons on the central cobalt and $\langle \hat{S}^2 \rangle = 0.83$ ¹⁴ show a partial broken symmetry character in a ‘desperate’ attempt of the variational principle to minimize the energy towards the truly multiconfigurational ground state, which is, however, impossible within the restrictions imposed by a single determinantal wavefunction. Hence the electronic structure¹⁴ of the complex has been studied based on the multiconfigurational spectroscopy oriented configurational interaction (SORCI) calculation. The ground state electronic configuration as obtained from the SORCI calculation on the $[\text{Co}(\text{L}_{\text{NN}})_2]$ complex is $(1a_g)^2(2a_g)^2(1b_{3g})^2(1a_u)^2(1b_{2g})^2(1b_{1u})^2(2b_{3g})^1(2b_{2g})^0(1b_{1g})^0$. D_{2h} symmetry is also considered for the complex and the same molecular orbital picture, as shown in Fig. 5 for the $[\text{Co}(\text{L}_2)]^{-}$ complex, results for the $[\text{Co}(\text{L}_{\text{NN}})_2]$ complex with the exception that the ligand orbitals now consist of nitrogen $2p$ orbitals instead of sulfur $3p$ orbitals. In the calculation three doubly occupied $(1a_g(d_{x^2-y^2}), 2a_g(d_z), 1b_{2g}(d_{xz}))$ and one singly occupied $(1b_{3g}(d_{yz}))$ molecular orbitals, are found to be predominantly of metal-d origin¹⁴ and hence, the valence state of the metal is best represented as d^7 Co^{II} ion. Interestingly, in contrast to the $[\text{Co}(\text{L}_2)]^{-}$ complex, where the $2b_{2g}$ orbital contains equal metal and ligand character, the $2b_{2g}$ orbital in $[\text{Co}(\text{L}_{\text{NN}})_2]$ is predominantly ligand based.¹⁴ Moreover, the SORCI many-electron ground state wavefunction contains $\sim 7\%$ of the double excitation $(1b_{1u})^2 \rightarrow (2b_{2g})^2$ which describes the diradical character of the ligand and rules out the alternative of ferromagnetic coupling between the ligands and antiferromagnetic coupling to the central metal. Thus in $[\text{Co}(\text{L}_{\text{NN}})_2]$ the lower effective nuclear charge of the ligand indeed facilitates a ligand based chemistry, and its electronic structure can be best represented as $[\text{Co}^{\text{II}}(\text{L}_{\text{NN}}^{\cdot-})_2]$, where a $\text{Co}(\text{II})$ ion is attached to two antiferromagnetically coupled ligand radicals.

B. Spectroscopic properties

1. EPR spectroscopy. $[\text{Co}^{\text{II}}(\text{L}_{\text{NN}}^{\cdot-})_2]$ possess a $S = 1/2$ ground state and hence is characterized by EPR. The EPR spectrum of $[\text{Co}^{\text{II}}(\text{L}_{\text{NN}}^{\cdot-})_2]$ with $g_x = 1.9906$, $g_y = 2.0508$, $g_z = 2.8100$ ($g_{\text{iso}} = 2.2838$) and ^{59}Co hyperfine coupling constants $A_{xx} = 24.0$, $A_{yy} = 0$, $A_{zz} = 42\text{ G}$ (line width $W_x = 20\text{ G}$, $W_y = 37\text{ G}$, $W_z = 38\text{ G}$) indicates that the unpaired electron resides in a metal d orbital.¹⁴ This is consistent with the $\text{Co}(\text{II})$ assignment of the complex. The spectroscopy oriented configuration interaction (SORCI) *ab initio* calculation (see below) rationalizes the large g_z shift (deviation of g_z from the free electron value of 2.0023) in the complex as the result of spin orbit coupling of the ground state with extremely low lying dipole forbidden ligand field excited states.¹⁴ The presence of near-orbital degeneracy is also proved by the fact that subtle variations (by adding an axial ligand or substituting one of the nitrogens by oxygen)¹⁴ in the ligand field strength in the complex shows large influence on the g_z shift.

2. MCD spectroscopy and assignment of transitions. In order to detect the individual transition, following the usual procedure, the low temperature MCD and room temperature absorption spectra for the $[\text{Co}^{\text{II}}(\text{L}_{\text{NN}}^{\cdot-})_2]$ complex have been subjected to a Gaussian deconvolution in the range $25\,000\text{--}5000\text{ cm}^{-1}$, which

gives rise to a total of 11 detectable transitions (bands 3–13 in Fig. 15) for the complex below $25\,000\text{ cm}^{-1}$.

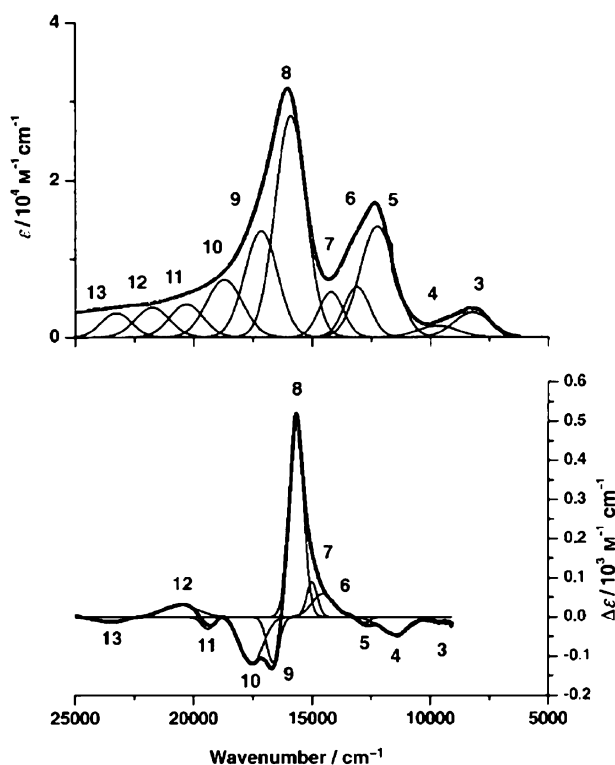


Fig. 15 Deconvoluted electronic absorption spectrum of $[\text{Co}^{\text{II}}(\text{L}_{\text{NN}}^{\bullet 1-})_2]^0$ (top) and its magnetic circular dichroism spectrum (below) recorded at 1.8 K and 5.0 T. Reproduced with permission from ref. 14.

The C/D ratios of all bands (with the exception of band 4) are ≤ 0.01 , indicating that the MCD spectrum is not dominated by transitions of d–d character, which would require C/D ratios ≥ 0.03 (ref. 14). The calculated absorption spectrum for the $[\text{Co}^{\text{II}}(\text{L}_{\text{NN}}^{\bullet 1-})_2]$ complex based on SORCI¹⁴ is found to be in well agreement with the experiment demonstrating the authenticity of the calculation.

The most intense transition in the $[\text{Co}^{\text{II}}(\text{L}_{\text{NN}}^{\bullet 1-})_2]$ complex should correspond to the transition $1b_{1u} \rightarrow 2b_{2g}$ which is a ligand-to-ligand charge transfer (since both the $1b_{1u}$ and $2b_{2g}$ orbitals are predominantly ligand based in $[\text{Co}^{\text{II}}(\text{L}_{\text{NN}}^{\bullet 1-})_2]$) transition of A_u symmetry and is allowed in x-polarization (along the long axis of the complex, see Fig. 10). In the case of the neutral cobalt complex this transition leads from a doubly occupied MO ($1b_{1u}$) to a virtual MO ($2b_{2g}$). Thus, in the excited state there are three unpaired electrons which can spin couple to two doublet and one quartet state. The absorption intensity for the quartet state will be very low since it is spin forbidden. Formally, the first doublet arises from the straightforward $1b_{1u} \rightarrow 2b_{2g}$ singlet excitation while the second excitation involves the $1b_{1u} \rightarrow 2b_{2g}$ triplet excitation with a concomitant spin flip of the unpaired electron in the $2b_{3g}$ SOMO. Thus, the second doublet is referred to as a ‘trip-doublet’ in Gouterman’s nomenclature³⁶ and formally corresponds to a double excitation. However, the two doublets are interacting through the Hamiltonian operator and can therefore mix and both acquire absorption intensity. Based on the SORCI calculation the bands 3 and 8 in the optical spectrum of the $[\text{Co}^{\text{II}}(\text{L}_{\text{NN}}^{\bullet 1-})_2]$

complex are assigned¹⁴ to the two components of the $1b_{1u} \rightarrow 2b_{2g}$ transition, with the lower energy transition corresponding to trip doublet³⁶ component. C/D ratio of band 3 (trip-doublet component) is very low (Table 4 in ref. 14) as may be expected from its relatively large double excitation character. The remaining bands 4–7 are assigned to LMCT or d–d transitions, which have a complicated origin, and involve double or even triple (band 5) excitations.¹⁴ Such excitations can only be crudely modeled in DFT and demonstrates the importance of an unbiased multireference approach as in SORCI. The transitions beyond band 8 are all of complicated nature and involve low lying double excitations (from SORCI) and were not analyzed in detail. In the SORCI calculation low lying excited d–d states below 2000 cm^{-1} , which are beyond the detection range of absorption and MCD experiments, are also predicted¹⁴ which explain the very large g_{max} shift observed in the EPR experiments for the $[\text{Co}^{\text{II}}(\text{L}_{\text{NN}}^{\bullet 1-})_2]$ ¹⁴ complex.

4. Conclusion

The most important goal of this present review is to establish the importance of a detailed spectroscopic and theoretical investigation, in order to make an unambiguous assignment of the, otherwise complicated, electronic structure of transition metal complexes involving non-innocent ligands. The complexes considered in this study are characterized by various spectroscopic methods like MCD, absorption, resonance Raman, EPR, and sulfur K-edge XAS. A theoretical model for the electronic structure of the complexes is then proposed based on DFT or *ab initio* methods, which can nicely explain the observed trends in the experimental spectra (MCD, rR, and abs, and EPR) of the complexes. Based on our studies the benzene dithiolato ligand is found to be readily one-electron oxidized yielding the dithiobenzosemiquinonato ($1-$) radical ion. The spectroscopic marker for such coordinated radicals is the presence of ligand-to-ligand (LLCT) intense charge transfer bands in the near infrared region in the absorption spectra and the resonance enhancement of the C–S stretch at $\sim 1100\text{ cm}^{-1}$ in the rR spectra upon exciting in the LLCT region. The non-innocent nature of the dithiolene ligand in any complex is however, strongly dependent on the nature of the transition metal ion present in the complex. Thus for the isoelectronic $[\text{M}^{\text{II}}(\text{L}^{2-})(\text{L}^{\bullet 1-})]^{-}$ ($\text{M} = \text{Ni}, \text{Pd}$ and Pt) or $[\text{Au}^{\text{III}}(\text{L}^{2-})(\text{L}^{\bullet 1-})]$ complexes involving a d^8 $\text{M}(\text{II})$ ($\text{M} = \text{Ni}, \text{Pd}$ and Pt) or Au^{III} ion attached to both the dithiolato ($2-$) and dithiobenzosemiquinonato ($1-$) forms of the ligand, the radical character (or the ligand character in the $2b_{2g}$ level) decreases in the order $[\text{Au}^{\text{III}}(\text{L}^{2-})(\text{L}^{\bullet 1-})] > [\text{Pd}^{\text{II}}(\text{L}^{2-})(\text{L}^{\bullet 1-})]^{-} > [\text{Pt}^{\text{II}}(\text{L}^{2-})(\text{L}^{\bullet 1-})]^{-} > [\text{Ni}^{\text{II}}(\text{L}^{2-})(\text{L}^{\bullet 1-})]^{-}$. This is reflected in the blue shift of the $1b_{1u} \rightarrow 2b_{2g}$ IVCT band on going from the Au to the Pd, Pt and to the Ni complexes (Fig. 11). This lowering of radical character on going from the Au to the Ni complex is attributed to the variation in the d orbital energies relative to the ligand, which in turn is dependent on the Z_{eff} and the relativistic potential³⁵ that mainly influences the energetic position of the d-shell at the central metal ion. The situation may be explained in a simple way by reference to Fig. 16, where the calculated energy of the metal d_{xz} orbital relative to the ligand $\pi^*_{-b_{2g}}$ orbital energy is plotted for the different bis(dithiolene) transition metal complexes considered in this review. Due to the high effective nuclear charge of the $\text{Au}(\text{III})$ ion the metal d_{xz} orbital in $[\text{Au}^{\text{III}}(\text{L}^{2-})(\text{L}^{\bullet 1-})]$ is situated very deep

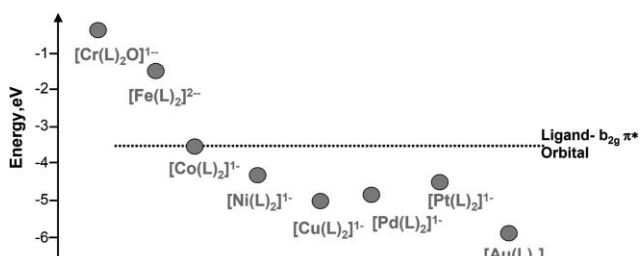


Fig. 16 Calculated energy of the metal d_{zx} orbital relative to the ligand π^* - b_{2g} orbital energy for the different complexes in the $[M(L)_2]^{n-}$ series.

in energy so that the metal–ligand mixing is minimum, providing maximum ligand character ($\sim 60\%$ S 3p character in the SOMO from ref. 15e) to the complex. In the corresponding $[Co(L)_2]^{1-}$ complex, however, the Co d_{zx} orbital is situated at a comparable energy to the ligand orbital providing considerable metal–ligand mixing in the $2b_{2g}$ SOMO (45% S 3p character from ref. 15a). Thus, as deduced from extensive previous studies,^{15a} an ambiguous case is met in $[Co(L)_2]^{1-}$ in which the oxidation state of the central cobalt cannot be unambiguously assigned. For all metals before Co in the first-row transition metal series, the metal d_{zx} orbital is predicted to be at a higher energy than the ligand orbital. Metal based redox processes are thus expected and observed for the $[Fe^{II}(L^2-)_2]^{2-15a}$ and $[Cr^V O(L^2-)_2]^{1-15f}$ complexes. The only reason that the redox chemistry does not occur in the case of $[Cu(L)_2]^{1-}$ is the electron count—the acceptor d_{zx} orbital is filled in the case of a Cu^{III} with a d^8 -configuration and the only possible acceptor orbital at the copper, the d_{xy} based b_{1g} orbital, is energetically inaccessible. Thus, despite the high effective nuclear charge of the central Cu^{III} oxidation of the ligand does not occur. In $[Co^{II}(L_{NN}^{*1-})_2]$ the ligand orbitals which were at comparable energies with the Co (3d) orbitals in $[Co(L)_2]^{1-}$, are now moved to higher energy due to lower effective nuclear charge of the ligand. This results in a predominantly ligand based chemistry in $[Co^{II}(L_{NN}^{*1-})_2]$.

Taken together, we believe that the results summarized here provide detailed insight into the covalencies and bonding descriptions of transition metal complexes involving non-innocent ligands like dithiolenes and phenylenediamines. We hope that these insights will prove useful in further characterizing the biological Mo- and W-dithiolenes and biologically relevant model complexes, and therefore help to address the questions of whether the ligands, in such compounds, could possibly act as non-innocent ligands which would certainly have significant implications for the reactivity of such sites.

Acknowledgements

We are grateful to the Fonds der Chemischen Industrie for financial support. K. R and T. P thank the Max-Planck Society for a stipend.

References

- (a) B. A. Jadzewski and W. B. Tolman, *Coord. Chem. Rev.*, 2000, **200**, 633; (b) P. Chaudhuri and K. Wieghardt, *Prog. Inorg. Chem.*, 2001, **50**, 151.
- (a) H. S. A. Sigel, *Metalloenzymes involving Amino Acid Residue and Related Radicals*, Marcel Dekker, New York, 1994; (b) J. Stubbe and W. A. Van der Donk, *Chem. Rev.*, 1998, **98**, 705.
- C. G. Pierpont and C. W. Lange, *Prog. Inorg. Chem.*, 1994, **41**, 331.

- D. Herebian, K. E. Wieghardt and F. Neese, *J. Am. Chem. Soc.*, 2003, **125**, 10997.
- U. Beckmann, E. Bill, T. Weyhermüller and K. Wieghardt, *J. Inorg. Biochem.*, 2001, **86**, 141.
- (a) P. Chaudhuri, C. N. Verani, E. Bill, E. Bothe, T. Weyhermüller and K. Wieghardt, *J. Am. Chem. Soc.*, 2001, **123**, 2213; (b) H. P. Chun, T. Weyhermüller, E. Bill and K. Wieghardt, *J. Inorg. Biochem.*, 2001, **86**, 182; (c) H. Chun, C. N. Verani, P. Chaudhuri, E. Bothe, E. Bill, T. Weyhermüller and K. Wieghardt, *Inorg. Chem.*, 2001, **40**, 4157; (d) H. Chun, T. Weyhermüller, E. Bill and K. Wieghardt, *Angew. Chem., Int. Ed.*, 2001, **40**, 2489; (e) H. Chun, E. Bill, E. Bothe, T. Weyhermüller and K. Wieghardt, *Inorg. Chem.*, 2002, **41**, 5091; (f) H. P. Chun, P. Chaudhuri, T. Weyhermüller and K. Wieghardt, *Inorg. Chem.*, 2002, **41**, 790; (g) D. Herebian, E. Bothe, E. Bill, T. Weyhermüller and K. Wieghardt, *J. Am. Chem. Soc.*, 2001, **123**, 10012; (h) D. Herebian, P. Ghosh, H. Chun, E. Bothe, T. Weyhermüller and K. Wieghardt, *Eur. J. Inorg. Chem.*, 2002, 1957.
- (a) P. Ghosh, E. Bill, T. Weyhermüller, F. Neese and K. Wieghardt, *J. Am. Chem. Soc.*, 2003, **125**, 1293; (b) F. Neese, *J. Phys. Chem. Solids*, 2004, **65**, 781.
- D. Herebian, E. Bothe, F. Neese, T. Weyhermüller and K. E. Wieghardt, *J. Am. Chem. Soc.*, 2003, **125**, 9116.
- X. R. Sun, H. Chun, K. Hildenbrand, E. Bothe, T. Weyhermüller, F. Neese and K. Wieghardt, *Inorg. Chem.*, 2002, **41**, 4295.
- (a) S. Bhattacharya, P. Gupta, F. Basuli and C. G. Pierpont, *Inorg. Chem.*, 2002, **41**, 5810; (b) W. Kaim, M. Wanner, A. Knodler and S. Zalis, *Inorg. Chim. Acta*, 2002, **337**, 163; (c) S. Frantz, H. Hartmann, N. Doslik, M. Wanner, W. Kaim, H. J. Kummerer, G. Denninger, A. L. Barra, C. Duboc-Toia, J. Fiedler, I. Ciofini, C. Urban and M. Kaupp, *J. Am. Chem. Soc.*, 2002, **124**, 10563; (d) W. Kaim, A. Dogan, M. Wanner, A. Klein, I. Tiritiris, T. Schleid, D. J. Stufkens, T. L. Snoeck, E. J. L. McInnes, J. Fiedler and S. Zalis, *Inorg. Chem.*, 2002, **41**, 4139; (e) C. G. Pierpont, *Inorg. Chem.*, 2001, **40**, 5727; (f) C. G. Pierpont, *Coord. Chem. Rev.*, 2001, **219**, 415; (g) C. G. Pierpont, *Coord. Chem. Rev.*, 2001, **216**, 99; (h) M. Glockle, K. Hubler, H. J. Kummerer, G. Denninger and W. Kaim, *Inorg. Chem.*, 2001, **40**, 2263; (i) G. A. Abakumov, V. K. Cherkasov, V. I. Nevodchikov, V. A. Kuropatov, G. T. Yee and C. G. Pierpont, *Inorg. Chem.*, 2001, **40**, 2434; (j) C. G. Pierpont and A. S. Attia, *Collect. Czech. Chem. Commun.*, 2001, **66**, 33.
- (a) B. S. Lim, D. V. Fomitchev and R. H. Holm, *Inorg. Chem.*, 2001, **40**, 4257; (b) D. V. Fomitchev, B. S. Lim and R. H. Holm, *Inorg. Chem.*, 2001, **40**, 645.
- (a) D. M. Adams, L. Noodleman and D. N. Hendrickson, *Inorg. Chem.*, 1997, **36**, 3966; (b) H. Sugiyama, G. Aharonian, S. Gambarotta, G. P. A. Yap and P. H. M. Budzelaar, *J. Am. Chem. Soc.*, 2002, **124**, 12; (c) P. H. M. Budzelaar, B. de Bruin, A. W. Gal, K. Wieghardt and J. H. van Lenthe, *Inorg. Chem.*, 2001, **40**, 4649; (d) P. H. M. Budzelaar, B. De Bruin, A. W. Gal, J. H. Van Lenthe and K. Wieghardt, *Abstr. Pap. Am. Chem. Soc.*, 2001, **221**, 444; (e) A. Bencini, C. A. Daul, A. Dei, F. Mariotti, H. Lee, D. A. Shultz and L. Sorace, *Inorg. Chem.*, 2001, **40**, 1582; (f) M. A. Blomberg and P. E. M. Siegbahn, *Mol. Phys.*, 1999, **96**, 571.
- C. Lauterbach and J. Fabian, *Eur. J. Inorg. Chem.*, 1999, 1995.
- E. Bill, E. Bothe, P. Chaudhuri, K. Chlopek, D. Herebian, S. Kokatam, K. Ray, T. Weyhermüller, F. Neese and K. Wieghardt, *Chem.–Eur. J.*, 2004, **11**, 204.
- (a) K. Ray, A. Begum, T. Weyhermüller, S. Piligkos, F. Neese and K. Wieghardt, *J. Am. Chem. Soc.*, 2005, **127**, 4403; (b) K. Ray, E. Bill, T. Weyhermüller and K. Wieghardt, *J. Am. Chem. Soc.*, 2005, **127**, 5641; (c) K. Ray, T. Weyhermüller, A. Goossens, M. W. J. Craje and K. Wieghardt, *Inorg. Chem.*, 2003, **42**, 4082; (d) T. Petrenko, K. Ray, K. Wieghardt and F. Neese, *J. Am. Chem. Soc.*, 2006, **128**, 4422; (e) K. Ray, T. Weyhermüller, F. Neese and K. Wieghardt, *Inorg. Chem.*, 2005, **44**, 5345; (f) R. Kapre, K. Ray, I. Sylvestre, T. Weyhermüller, S. DeBeer George, F. Neese and K. Wieghardt, *Inorg. Chem.*, 2006, **45**, 3499.
- (a) G. N. Schrauzer, *Transition Met. Chem. (NY)*, 1968, **4**, 299; (b) J. A. McCleverty, *Prog. Inorg. Chem.*, 1968, **10**, 49; (c) R. H. Holm and M. J. O'Connor, *Prog. Inorg. Chem.*, 1971, **14**, 241; (d) R. Eisenberg, *Prog. Inorg. Chem.*, 1970, **12**, 295; (e) H. B. Gray, *Transition Met. Chem. (NY)*, 1965, **1**, 240; (f) *Dithiolene Chemistry*, E. I. Stiefel, (Ed.), *Prog. Inorg. Chem.*, 2004, Vol **52**; (g) V. Bachler, G. Olbrich, F. Neese and K. Wieghardt, *Inorg. Chem.*, 2002, **41**, 4179; (h) D. Sellmann, H. Binder, D. Häussinger, F. W. Heinemann and J. Sutter, *Inorg. Chim. Acta*, 2000, **300**, 829; (i) K. Mrkvova, J. Kamení, Z. Sindela and L. L. Kvitěk, *Transition Met. Chem.*, 2004, **29**, 238; (j) D. T. Sawyer, G. S. Srivatsa,

- M. E. Bodini, W. P. Schaefer and R. M. Wing, *J. Am. Chem. Soc.*, 1986, **108**, 936; (k) E. I. Stiefel, J. H. Waters, E. Billig and H. B. Gray, *J. Am. Chem. Soc.*, 1965, **87**, 3016; (l) A. L. Balch and R. H. Holm, *J. Am. Chem. Soc.*, 1966, **88**, 5201; (m) S.-M. Peng, C.-T. Chen, D.-S. Liaw, C.-I. Chen and Y. Wang, *Inorg. Chim. Acta*, 1985, **101**, L31; (n) A. Earnshaw, *Introduction to Magnetochemistry*, Academic Press, London, 1968.
- 17 (a) C. Enroth, B. T. Eger, K. Okamoto, T. Nishino, T. Nishino and E. F. Pai, *Proc. Natl. Acad. Sci. U. S. A.*, 2000, **272**, 1599; (b) R. C. Bray, B. G. Malmström and T. Vännngard, *Biochem. J.*, 1959, **73**, 193; (c) R. Hille and T. Nishino, *FASEB J.*, 1995, **9**, 995; (d) R. Hille, *Chem. Rev.*, 1996, **96**, 2757; (e) W. Campbell, *Plant Physiol.*, 1996, **111**, 355; (f) L. P. Solomonson and M. P. Barber, *Plant Mol. Biol.*, 1990, **41**, 225; (g) H.-L. Li, C. Temple, K. V. Rajagopalan and H. Schindfelin, *J. Am. Chem. Soc.*, 2000, **122**, 7673; (h) R. Cammack and J. H. Weiner, *Biochemistry*, 1990, **29**, 8410; (i) P. Ellis, T. Conrads, R. Hille and P. Kuhn, *Structure*, 2001, **9**, 125; (j) G. L. Anderson, J. Williams and R. Hille, *J. Biol. Chem.*, 1992, **267**, 23674; (k) S. Mukund and M. W. W. Adams, *J. Biol. Chem.*, 1991, **266**, 14208.
- 18 (a) K. Wang and E. I. Stiefel, *Science*, 2001, **291**, 106; (b) J. T. Groves and W. J. Kruper, Jr, *J. Am. Chem. Soc.*, 1979, **101**, 7613; (c) E. G. Samsel, K. Srinivisan and J. K. Kochi, *J. Am. Chem. Soc.*, 1985, **107**, 7606; (d) K. Srinivasan and J. K. Kochi, *Inorg. Chem.*, 1985, **24**, 4671.
- 19 S. Boyde, S. R. Ellis, C.D. Garner and W. Clegg, *J. Chem. Soc., Chem. Commun.*, 1986, 1541.
- 20 R. K. Szilagy, B. S. Lim, T. Glaser, R. H. Holm, B. Hedman, K. O. Hodgson and E. I. Solomon, *J. Am. Chem. Soc.*, 2003, **125**, 9158.
- 21 (a) E. I. Solomon, B. Hedman, K. O. Hodgson, A. Dey and R. K. Szilagy, *Coord. Chem. Rev.*, 2005, **249**, 97; (b) S. E. Shadle, J. E. Penner-Hahn, H. J. Schugar, B. Hedman, K. O. Hodgson and E. I. Solomon, *J. Am. Chem. Soc.*, 1993, **115**, 767; (c) T. Glaser, B. Hedman, K. O. Hodgson and E. I. Solomon, *Acc. Chem. Res.*, 2000, **33**, 859.
- 22 (a) F. Neese, B. Hedman, K. O. Hodgson and E. I. Solomon, *Inorg. Chem.*, 1999, **38**, 4854; (b) B. Hedman, K. O. Hodgson and E. I. Solomon, *J. Am. Chem. Soc.*, 1990, **112**, 1643.
- 23 (a) D. M. Dooley and J. H. Dawson, *Coord. Chem. Rev.*, 1984, **60**, 1; (b) A. J. Thomson, M. R. Cheesman and S. K. George, *Methods Enzymol.*, 1993, **226**, 199; (c) M. R. Cheesman, C. Greenwood and A. J. Thomson, *Adv. Inorg. Chem.*, 1991, **36**, 201.
- 24 E. I. Solomon, E. G. Pavel, K. E. Loeb and C. Campochiaro, *Coord. Chem. Rev.*, 1995, **144**, 369.
- 25 (a) P. J. Stephens, *J. Chem. Phys.*, 1970, **52**(7), 3489; (b) P. J. Stephens, *Adv. Chem. Phys.*, 1975, **35**, 197; (c) P. J. Stephens, *Annu. Rev. Phys. Chem.*, 1974, **25**, 201; (d) A. D. Buckingham and P. J. Stephens, *Annu. Rev. Phys. Chem.*, 1966, **17**, 399.
- 26 S. B. Piepho and P. N. Schatz, *Group Theory in Spectroscopy with Applications to Magnetic Circular Dichroism*, John Wiley & Sons, New York, 1983.
- 27 C. H. Henry, S. E. Schnatterly and C. P. Slichter, *Phys. Rev.*, 1965, **137**(2A), A583.
- 28 (a) P. J. Stephens, *Chem. Phys. Lett.*, 1968, **2**(4), 241; (b) G. A. Osborne and P. J. Stephens, *J. Chem. Phys.*, 1972, **56**(1), 609.
- 29 A. A. Gewirth and E. I. Solomon, *J. Am. Chem. Soc.*, 1988, **110**, 3811.
- 30 F. Neese and E. I. Solomon, *Inorg. Chem.*, 1999, **38**, 1847.
- 31 M. D. Carducci, C. Brown, E. I. Solomon and J. H. Enemark, *J. Am. Chem. Soc.*, 1994, **116**, 11856.
- 32 As we move across the d-block from left to right, we are successively adding a proton and an electron at each step. The proton increases the nuclear charge by +1 e. The electron is added to one of the 3d orbitals. The d-orbitals have two nodes and therefore d-electrons shield the nuclear-charge rather poorly. Hence, the effective nuclear charge will rise steadily over the d-block and therefore d-orbitals will be stabilized. On moving down a group, again the increasing nuclear charge is not fully shielded by the d- or f-electrons and hence the outer d-orbitals are stabilized.
- 33 S. I. Gorelski, L. Basumallick, J. Vura-Weis, R. Sarangi, K. O. Hodgson, B. Hedman, K. Fujisawa and E. I. Solomon, *Inorg. Chem.*, 2005, **44**, 4947.
- 34 (a) A. C. Albrecht, *J. Chem. Phys.*, 1961, **34**, 1476; (b) J. Tang and A. C. Albrecht, In *Raman Spectroscopy, Theory and Practice*, ed. H. A. Szymanski, Plenum Press, New York, 1970, p. 33; (c) R. S. Czernuszewicz and T. G. Spiro, in *Inorganic Electronic Structure and Spectroscopy*, ed. E. I. Solomon and A. B. P. Lever, Wiley-Interscience, New York, 1999, vol. I, p. 353.
- 35 In heavy atoms the core electrons are subjected to substantial electrostatic fields due to the larger nuclear charge of the nucleus. As a result, they are pulled closer, to the nucleus, are bound tighter, and are confined to smaller volumes of space. Due to the Heisenberg uncertainty principle, restricting the electron to a smaller space results in a much higher radial velocity (approaching c , the speed of light) since we cannot know both position and speed precisely. According to Einstein's equation, as the velocity of an object approaches the speed of light, its mass increases with respect to its rest mass (K. Balasubramnium, *Relativistic effects in Chemistry, Part-A*. Wiley Interscience, 1997). Thus due to relativistic effects the core electrons in heavy metals are heavier than their rest mass, thus imparting significantly more kinetic energy to the particle. In terms of the simplified equation for the Bohr radius, there is a mass dependence in the denominator, thus causing the relativistic radius to be significantly lower than the non relativistic ones (P. Pyykkö and J.-P. Desclaux, *Acc. Chem. Res.*, 1979, **12**, 276). In heavy elements like Pt the inner s- and p-orbitals experience a direct relativistic orbital contraction and shrink in size. The effect on the d-orbitals is quite different, however; the probability of these electrons approaching close to the nucleus is exceedingly small. In fact, due to s- and p-contraction, the d orbitals are more effectively screened and thus see an indirect relativistic orbital expansion. They expand radially and increase in energy, thus being destabilised. Thus, on moving from Ni to Pd and to Pt there are two opposing effects determining the energy of the d-orbitals; the increasing effective nuclear charge which has a stabilising influence on the d-orbitals and increasingly strong relativistic effects which have a destabilizing effect on the d-orbitals. For Ni(II) and Pd(II) ions in $[M(L)_2]^{+}$ ($M = Ni$, and Pd) complexes the relativistic effect is not significant. However, for Pt(II) in $[Pt(L)_2]^{+}$ the effective nuclear charge and relativistic effects are of comparable magnitude which results in the Pt 5d-orbitals having an energy in between Ni-3d and Pd-4d. In $[Au(L)_2]^{+}$, the +3 charge in Au(III) ion stabilizes the 5d-orbitals to a large extent. Although the relativistic effects destabilizes the 5d-orbitals to a certain extent, the energy of the 5d orbitals in Au(III), still remains much lower than in the Ni(II), Pd(II) or Pt(II) nd-orbitals.
- 36 (a) M. G. Cory and M. C. Zerner, *Chem. Rev.*, 1991, **91**, 813; (b) M. Gouterman, *J. Mol. Spectrosc.*, 1961, **6**, 138.